Received: 2023-01-13 | Accepted: 2022-03-10 | Published: 2023-07-12

A Droplet of Liquid Steel: Prills in Crucible Steel Production Remains

Meghna Desai, Sriperumbudur Jaikishan and Thilo Rehren

Keywords
Crucible prills, steel prills, steel ingots, phosphorus, silicon, Telangana, Merv, crucible steel

Abstract

The formation of steel prills is evident from all crucible steel production ceramics. The paucity of crucible steel ingots in the archaeological record means that the full production *chaîne opératoire* remains incompletely known and partly speculative. Here, we use the analysis of prills from crucible slags and crucibles to explore the composition of the missing ingots and to learn more about their formation conditions. To test the correlation of prill compositions with the ingots and/or the crucible ceramic, we examined prills formed in two different crucible types - ferruginous and non-ferruginous, used in Telangana (India) and Merv (Turkmenistan) crucible steel production, respectively. Both crucible types, when fired at high temperatures under reducing conditions, form prills across the crucible profile, i.e. in the outer fuel ash glaze, the crucible body and the inner crucible slag. Ferruginous crucibles from Telangana showed abundant, pronounced and relatively large prills as compared to the iron-poor kaolinitic crucibles of Merv. Factors including the clay selection and addition of various tempers, fuel ash and crucible charge all showed an influence on the prill composition. Using SEM-EDS as our analytical tool, we discuss the factors that influence the alloying elements in prills, the prill microenvironments and their potential relationship to the corresponding ingots.

Introduction

Crucible steel production[1] is one of the most technologically demanding early metallurgical processes, operating at temperatures of up to 1300 to 1350 °C in ceramic crucibles and under fiercely reducing conditions (Lowe, 1989; Srinivasan and Griffiths, 1997; Juleff, 1998; Feuerbach, 2002; Juleff, Srinivasan and Ranganathan, 2011; Balasubramaniam, Pandey and Jaikishan, 2007; Rehren and Papakhristu, 2003; Alipour and Rehren, 2014; Güder, et al., 2022; Alipour and Rehren, 2023 etc.).

Accordingly, alumina-rich refractory clays were commonly used to produce these crucibles, consisting of the crucible bodies, typically of cylindrical shape and a closely fitting lid to ensure minimal gas exchange between the crucible contents and the surrounding furnace atmosphere; the necessary pressure release was achieved either through a porous ceramic body, or carefully applied small openings in the lids (Rehren and Papachristou, 2003, p.400). Differences exist in the choice of additives in the clay, such as crushed silica and grog (Merv: Feuerbach, 2002; Chāhak: Alipour, 2017), charcoal and straw (Kubadabad: Güder, et al., 2022), or rice husk and quartz (south-central and southern India: e.g., Lowe, Merk and Thomas, 1990), to further improve the thermal and structural properties of the ceramic. In certain naturally available high performance refractory kaolinitic clays, no modifications were required (Akhsiket: Rehren and Papakhristu, 2000) to produce crucibles.

Crucible steel-making crucibles are invariably fired from the outside (Bayley and Rehren, 2007) and set in groups in furnaces (Voysey, 1832; Craddock, 1998), regardless of the actual process, whether carburisation of bloomery iron with organic matter, co-fusion of bloomery and cast iron, or decarburisation of cast iron. This setting implies that the temperature within the crucible is effectively the same as on its outside, while the chemical environment, particularly the redox conditions can vary between the furnace chamber, the body of the ceramic vessels and the inside of the crucibles. During firing, the crucible fabrics undergo several phase and compositional changes and interact on their inside with the charge and on the outside with the furnace environ-

DOI:10.46586/metalla.v27.2023.i1.55-80

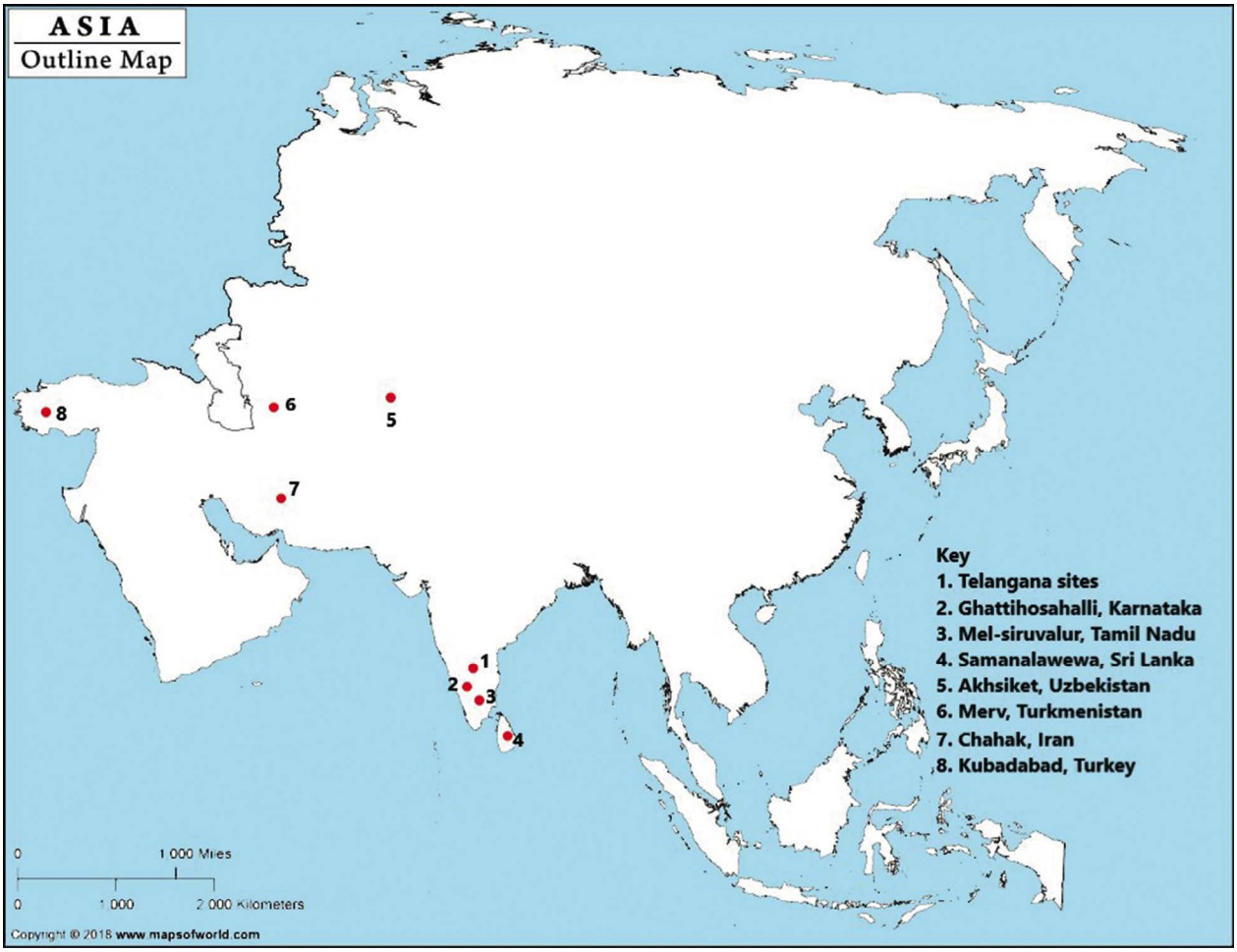

Figure 1. Map of crucible steel production sites in Asia, as referred in the text (modified from mapsofworld). Illustration: https://www.mapsofworld.com/, modified by M. Desai and Th. Rehren, The Cyprus Institute.

ment. By the end of the process, the ingots are retrieved and the crucibles discarded. At this stage, the crucible body consists of three distinct parts: the inner crucible slag, the crucible body and the outer fuel ash glaze (hereafter FAG).

Metallic iron prills form in the matrices of the crucibles, as reported in most crucible steel production studies (Srinivasan, 1994; Feuerbach, 2002; Alipour, 2017; Güder, et al., 2022). As first reported in the seminal study by Freestone and Tite (1986) on southern Indian crucible fragments, iron oxide from the ferruginous ceramic is reduced to metallic iron prills at high temperature. In the early 2000s, prills were also reported from crucible steel produced in non-ferruginous kaolinitic crucibles from Merv (Feuerbach 2002). In the absence of ingots, prills were analysed by electron microscopy for their composition and microstructure, assumed to be representative of the ingot microstructure and composition (Feuerbach, 2002; Alipour, 2017).

We explored two case studies representing crucible steel production using iron-rich ceramics from Telangana and iron-poor ceramics from Merv, Turkmenistan, respectively. This selection serves to compare the reaction of these two fundamentally different types of fabrics to the process conditions, in order to test whether the fabric type has an effect on the prill formation, and how this shows in the prill compositions. The specific sites were selected for the availability of material. We analysed prills formed in these crucibles to understand the effect of ceramic composition and firing environment on prill formation, vis-à-vis the formation of prills from the charge alone. We discuss the common denominators leading to the formation of these prills, such as high firing temperatures, crucible ceramic composition, strongly reducing redox conditions and availability of alloying elements to reconstruct an important aspect of the production parameters. The aforementioned factors provide a unique compositional character to each prill, thus showing high variability, due to localised compositional differences, the effect of carbon-controlled reactions, fuel selection, and clay preparation. The current study was undertaken to see whether the prills in the different layers differ from each other, and explore the information potential of metallic iron prill formation in

crucible steel ceramics, particularly the degree to which micro-conditions within the different parts of crucibles vary, and what these variations represent.

Problem and potential

It has long been known that metal prills form in one or more of the three crucible parts (Freestone and Tite, 1986, pp.53-55; Lowe 1989). Under the high temperature reactions taking place at strongly reducing conditions, any reducible compounds, that is those that can be reduced to their metallic state using charcoal as the reducing agent (Dillmann and L'Héritier, 2007; Charlton, et al., 2012), within the charge, crucible fabric and FAG, respectively, are reduced and consolidate as prills. Although the prills are based primarily on iron, which by itself will not melt even at these high temperatures, the strongly reducing conditions ensure sufficient carbon is present to form steel and bring the melting temperature down by several hundred degrees Celsius (see Figure 2). The prills typically take the optimum spherical, droplet-like shape, embedded in a viscous silica-rich glassy melt that forms a protective bath (Pryce and Natapintu, 2009), thereby preventing re-oxidation of the prills. In contrast, the non-reducible compounds (NRCs) fractionate into the crucible slag and FAG melts. Despite significant interstitial melt formation, the crucible bodies retain enough of their crystalline structure to keep the vessel mechanically stable; this limits the mobility of the locally formed prills, resulting in no or very little coagulation to larger prills within the crucible body. Ongoing research has shown that several characteristics of these prills differ systematically between crucible slag, ceramic body and FAG, reflecting their different physio-chemical microenvironments. Understanding the conditions that affect the final prill composition therefore holds the potential to benefit the reconstruction of the process conditions under which they formed and to identify specific process parameters from crucible waste fragments.

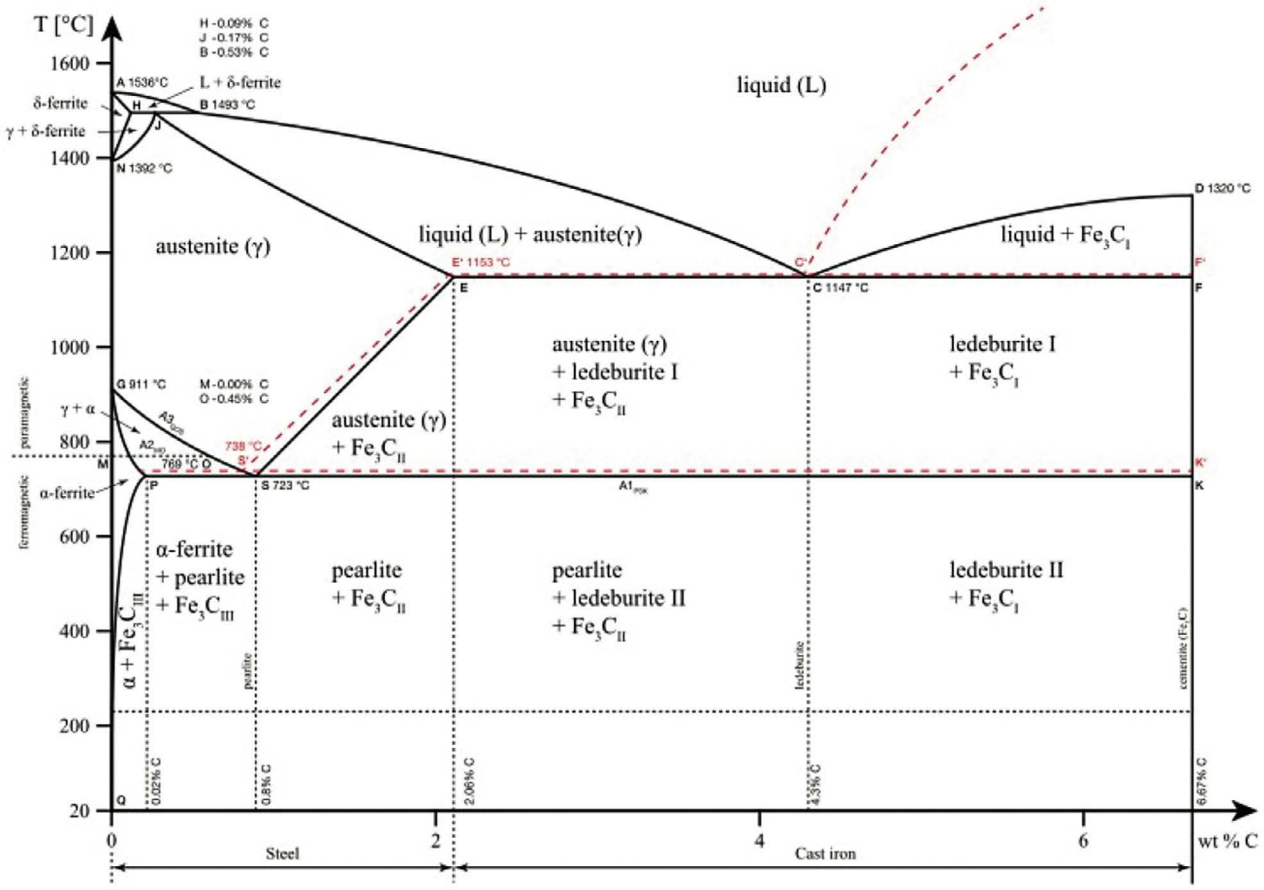

Figure 2. Iron-carbon phase diagram. The melting temperature of pure iron is around 1540 °C. As the carbon content in iron increases, the melting point decreases significantly. Thus, iron alloyed with 2 % carbon (steel) would begin to melt at around 1200 °C and be fully molten around 1450 °C (courtesy, AG Caesar, CC BY-SA 4.0 <https://creativecommons.org/licenses/by-sa/4.0>, via Wikimedia Commons). Illustration: AG Caesar, CC BY-SA 4.0 <https://creativecommons.org/licenses/by-sa/4.0>, via Wikimedia Commons.

Crucible slag and crucible slag film

The separation, melting and consolidation of the alloy and its impurities inside the crucible resulted in the formation of the crucible slag, which typically has a dark, translucent black appearance and floats on top of the liquid steel. The formation and composition of slag in historical crucible steel making in India are poorly studied. If the crucible charge consists of bloomery iron and organic matter, as in much of the southern Indian and Sri Lankan wootz making, the slag forms from a combination of any bloomery slag inclusions in the metal, the ash of the added organic matter and some contribution from the ceramic vessel. In contrast, Central Asian crucible steel making is characterised by the addition of significant amounts of mineral additives to the charge, resulting in much more slag formation (e.g., Rehren and Papakhristu, 2000). This has been well studied in the medieval Persian Chāhak crucibles, that hold significant amounts of crucible slag rich in prills including phosphorous, chromium and manganese from the crucible charge (Alipour, 2017, pp.316-319; Alipour and Rehren, 2021; 2023). Due to the intimate relationship between the crucible slag and the crucible steel ingot forming during the process, it is likely that the prills trapped in the crucible slag are compositionally close to the final ingot. Since the ingots are very rarely preserved (but see Jaikishan, Desai and Rehren, 2021 and Güder, et al., 2022), analysing the prills preserved in crucible slag gives an important window into the product of the process (Srinivasan, 1994; Feuerbach, 2002).

In addition to the crucible slag that solidifies above the ingot, a small part forms a film or layer between the crucible wall and the ingot; due to the shrinkage of the ingot when it solidifies at a temperature when the slag is still viscous, this film often develops a 'honeycomb' pattern in the lower half of the crucible walls. It has an intermediate composition between the main crucible slag and the crucible body and is exposed to its own microenvironment, being trapped between the bulk of the liquid steel and the ceramic body.

Ceramic body

The formation of metal prills in the ceramic body is prominent in crucibles made from ferruginous clay, as was the case in south-central and southern India, Chāhak and Kubadabad. During firing under reducing conditions, the iron oxide in the ceramic reduces to metallic iron prills, and therefore very little iron oxide remains in the bulk ceramic matrix, rendering it more refractory (Freestone and Tite, 1986). The presence of certain minerals in the ceramic body, such as ilmenite or apatite, may add to the composition of the body prills, while the semi-permeability of the ceramic prevents the formation of larger prills, even at high temperatures. In contrast, most Central Asian crucible steel-making ceramics have very little iron oxide and therefore prills are only sparsely present in their ceramic bodies, if at all.

Fuel ash glaze (FAG) and fuel ash slag (FAS)

During their use, the crucibles[2] are heated for extended periods of time in specific furnaces. Depending on the furnace design, the fuel ash can interact more or less with the ceramic on the outside of the crucibles. Due to the strongly fluxing properties of fuel ash, this results in the formation of a distinct and highly vitrified glaze-like layer. This FAG layer reflects the composition of the ceramic body and the fuel ash, therefore providing information about fuel sources, operation temperatures, raw materials and others.

Little is known about the fuel used to fire the crucible furnaces. During firing, the organic component of the fuel burns, whereas the inorganic component is released into the furnace environment either as solid ash, or as vapour. These inorganic components, primarily lime (CaO), magnesia (MgO), silica (SiO_2), potash (K_2O) and phosphate (P_2O_5) (Misra, Ragland and Baker, 1993; Stern and Gerber, 2004), interact with the outside of the crucibles and the inside of the furnace walls. Lime and potash are important fluxes, leading to vitrification of the ceramic. Fuel ash is also a considerable source of phosphorus and occasionally manganese; the composition of the fuel ash varies widely between different types of fuel, potentially opening the possibility to determine the type of fuel used from the composition of the FAG.

The FAG is a typically thin vitrified layer on a much thicker ceramic body; accordingly, the ceramic composition outweighs the fuel ash component in the FAG. In contrast, Fuel ash slag (FAS) forms greenish-grey chunks of slag with various levels of vitrification, much richer in FA and containing less ceramic material. We interpret this FAS to have formed in the crucible furnace during the prolonged firing, said often to last for several days, due to the accumulation of large amounts of fuel ash at the bottom of the furnace, where it absorbs relatively minor amounts of soil and ceramics. Thus, while the main components from which FAG and FAS form are the same linking the FAS to the FAG, they contain different proportions of technical ceramic. Several pieces of lose FAS from Telangana contained large metallic iron prills, which we include here as well.

Redox conditions

The chemical behaviour of the compounds in the presence of carbon monoxide gas at high temperature distinguishes them as reducible or non-reducible. The oxides or compounds that remain unreduced and/or are oxidized during the firing process are termed non-reducible compounds, or NRCs (Charlton, et al., 2012; Dillmann and L'Héritier, 2007). Oxides such as CaO, K_2O, MgO, Al_2O_3, etc. belong to this category. Transition metal oxides, e.g. FeO, CuO, PbO etc. are reducible under pre-industrial bloomery furnace conditions (Puigdollers, et al., 2017). In crucible steel making, however, more strongly reducing conditions and higher firing temperatures prevail, leading to an intermediate group of oxides, including SiO_2, MnO and Cr_2O_3, which on their own are non-reducible. However, these can be reduced to some extent and incorporated into the me-

Figure 3. Ellingham Diagram highlighting the reduction parameters of metal oxides. The oxides further down in the graph, such as SiO_2, TiO_2, Al_2O_3, MgO and CaO, are more stable and not easily reduced by carbon monoxide. Note the different slopes for the $2C+O_2 = 2CO$ buffer (red line) and the metal – metal oxide buffers, resulting in more likely reduction at higher temperatures (X-axis). Reduction of the oxide to the metal happens if the redox conditions are above the red line and below the metal – metal oxide line. The green line shows the estimated operating temperature for the crucible steel production, around 1300 °C (source: metallos, CC BY-SA 3.0 <https://creativecommons.org/licenses/by-sa/3.0>, via Wikimedia Commons). Illustration: metallos, CC BY-SA 3.0 <https://creativecommons.org/licenses/by-sa/3.0>, via Wikimedia Commons, modified by M. Desai and Th. Rehren.

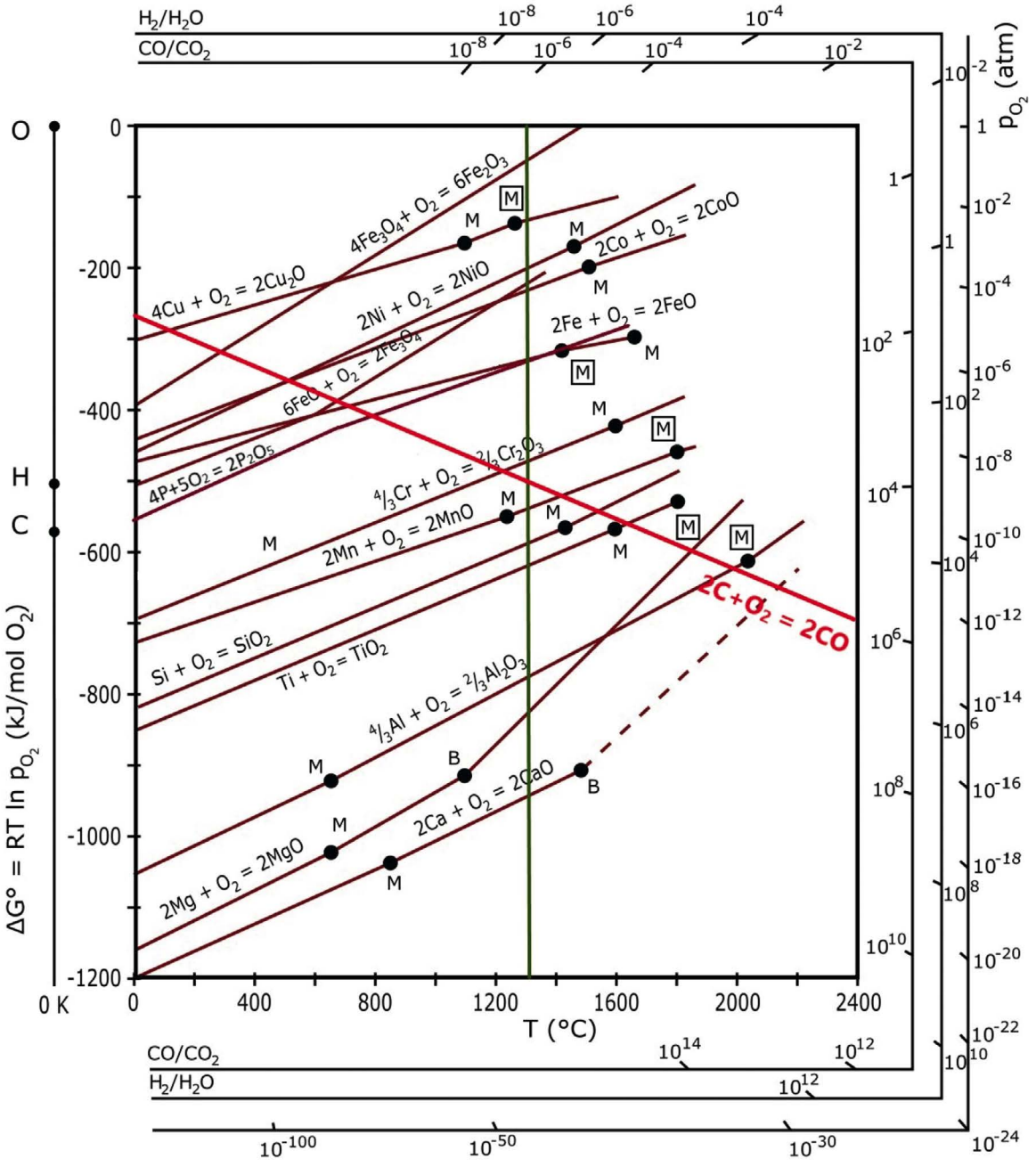

tallic phase in the presence of metallic iron (Rostoker and Bronson, 1990, pp.107-113), which acts as a sink and constantly removes the reduced metal from the equilibrium reaction.

Of these, SiO_2 is an omni-present compound, but often chemically bonded as silicate, which prevents easy reduction. However, in rice husk temper, where it is present as phytoliths of pure silica with a large surface area, it undergoes a carbothermic reaction with the disintegrating temper serving as the carbon source.

Iron-rich ceramic bodies

Northern Telangana landscape is well-known pre-industrial crucible steel production (Lowe, 1989; Lowe, Merk and Thomas, 1990; Jaikishan, 2007; Srinivasan, 1994; Juleff, Srinivasan and Ranganathan, 2011; Jaikishan, Desai and Rehren, 2021).

The crucibles here range from 2 to 12 cm in diameter (Lowe 1989); their profile consists of the outer FAG, the rice husk-tempered crucible body and the inner crucible slag film (Figures 4 and 5a-d). All three parts of the crucible profiles contain prills, as previously reported by Balasubramaniam, Pandey and Jaikishan (2007) and Girbal (2017). These metallic iron prills are alloyed with carbon and also phosphorus and/or silicon. The distribution and composition of these alloying elements vary greatly within and between the prills. As a general rule, FAG prills contain higher phosphorus; in the crucible body, the metallic prills contain silicon, phosphorus, or both and in the crucible slag and the crucible slag film the prills are typically alloyed with low to intermediate phosphorus compared to the FAG prills.

Previous work in iron-rich ceramic bodies

The seminal study by Freestone and Tite (1986) presents an understanding of the formation and role of iron prills in ferruginous crucible clays from Ghattihosahalli, southern India. Under strongly reducing conditions, ferruginous clays lead to the formation of metallic iron prills, leaving behind very little iron oxide in the fabric (about 1-3 wt.% oxide), compared to a bulk nominal iron oxide content of 6-8 wt.%. Shortly thereafter, Srinivasan (1994) reported a high phosphorus iron prill from crucible slag from Mel-siruvalur. Two other prills were analysed from the Mel-siruvalur crucible fabric showed no phosphorus elevation. Alipour (2017) and Alipour and Rehren (2021) reported metallic iron prills in the Chāhak crucible bodies from southern Iran, based also on ferruginous clays and various levels of phosphorus in prills in the FAG and the crucible slag fins; the latter also contained manganese and chromium. The phosphorus

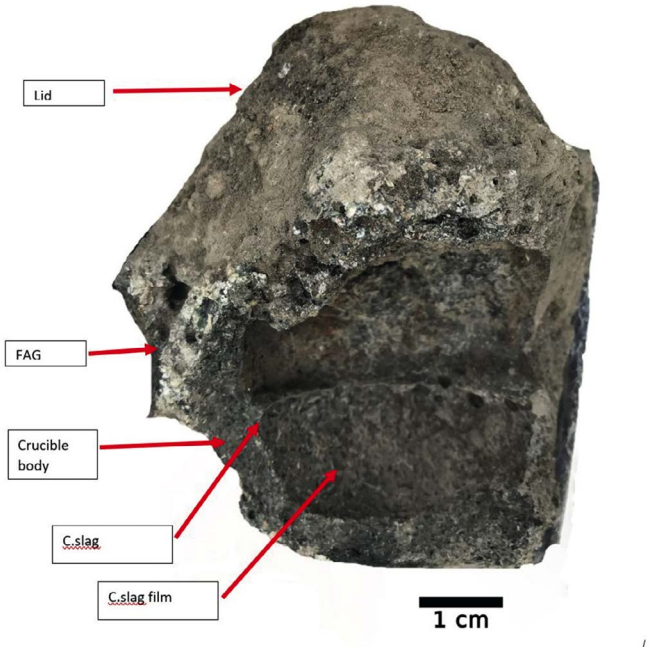

Figure 4. Semi-preserved crucible body fragment with lid luted on the top. FAG: fuel ash glaze, C.slag: crucible slag. Crucible from Konasamudram, India. Photo: M. Desai and Th. Rehren, Archaeological Science Laboratories, The Cyprus Institute.

content in the Chāhak FAG prills is higher in comparison to prills in the crucible body and crucible slag fin (Alipour, 2017, p.315).

Initial data from the early Islamic site of Essouk-Tadmekka in Mali shows ferruginous, organically tempered crucibles with high carbon prills of cast iron composition in the crucible slag, suggesting their use for crucible steel making (Rehren and Nixon, 2017, p.194). Most recently, Güder, et al. (2022) reported analytical data from Anatolian Seljuk period crucible steel making crucibles from Kubadabad in western Anatolia, which were also made from iron-rich clays. Here, the crucible slag is high in manganese dioxide; unfortunately, the composition of prills from the Kubadabad crucibles is currently unknown.

Iron-poor ceramic bodies

Several sites in Central Asia used white-firing, iron-poor ceramics for crucible steel making, among them Akhsiket in Uzbekistan and Merv in Turkmenistan. Here, we use material from Merv as a comparative case study. The Merv crucibles contained cast iron prills on the inner surface of the crucible body (Feuerbach, 2002), although they were not as numerous as they were in the Chāhak, Telangana, Ghattihosahalli and Kubadabad crucibles. To compare the nature and content of metallic iron prills, crucibles and crucible slag fins from Merv were systematically reanalysed with emphasis on the iron prills, using the same methodology and instrumentation as for the Telangana crucibles.

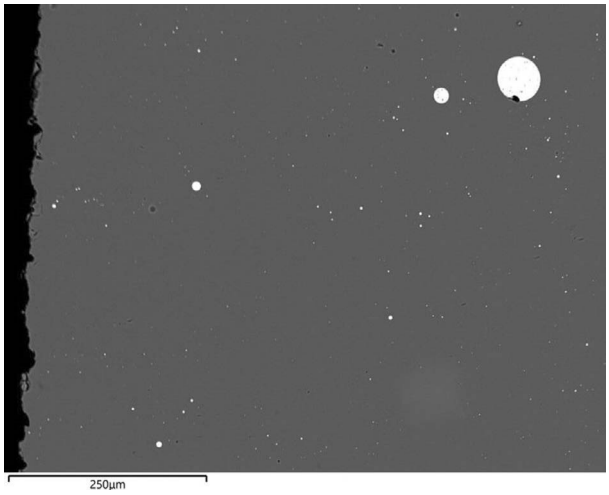

Figure 5a. Crucible slag, with metal prills in a glass matrix. Scale: 250 µm or 100 x.

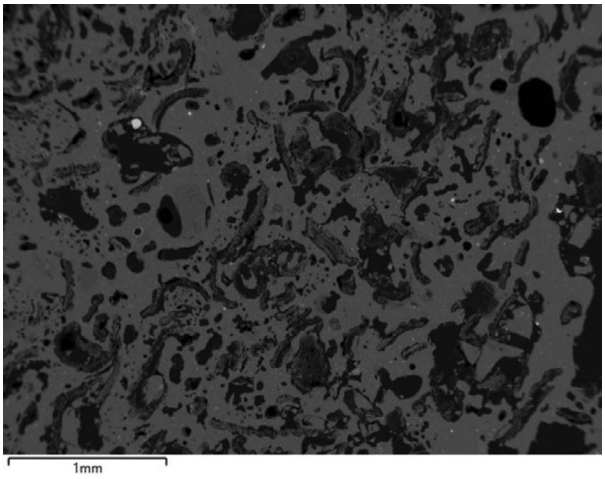

Figure 5b. Crucible body with rice husk temper and associated metal prills. Scale: 1mm or 25 x.

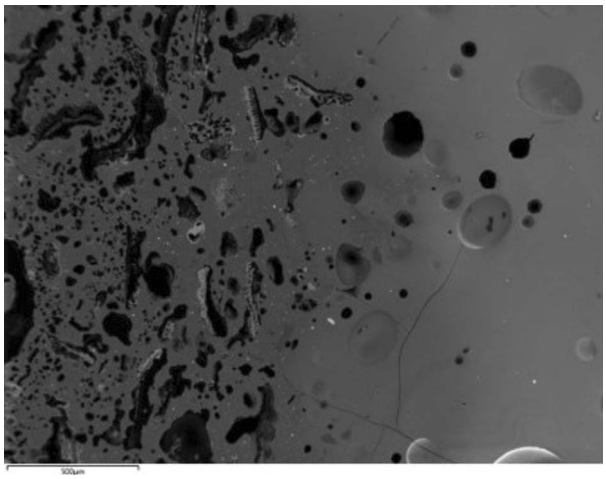

Figure 5c. Transition region between crucible body and FAG. Note the silica-rich phytoliths (grey) in the burnt-out temper cavities. Scale: 100 µm or 300 x.

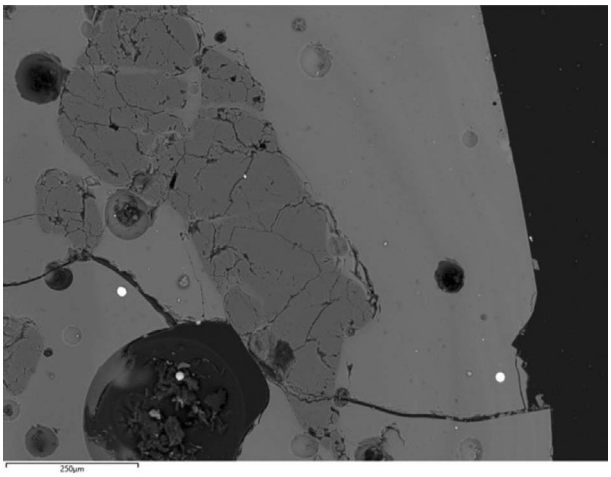

Figure 5d. FAG with large quartz grains (dark grey) and some metal prills. Scale: 250 µm or 100 x.

Figures 5a-d. A sequential overview of the crucible profile (from left to right): crucible slag, crucible body with rice husk temper, transition from body to FAG and FAG. Photos: M. Desai and Th. Rehren, Archaeological Science Laboratories, The Cyprus Institute.

Materials and methods

For this study, we selected crucible fragments that showed several of the compositional layers described above, representing both small and large vessels, where available. The crucible steel production waste from Telangana includes broken crucibles, lose fragments of crucible slags and FAS. The samples were prepared as polished blocks following standard procedures for Optical Microscopy (OM) and Scanning Electron Microscopy with Energy-Dispersive Spectromery (SEM-EDS) analysis, finishing with a final polish using 1 µ diamond paste. During sample selection, the FAG, FAS, crucible slag, crucible body and bases of the lids were probed for any projecting larger prills. Three such prills were isolated from Telangana crucibles, one from crucible slag, one from FAG/S and one from the base of a lid. The remaining prills were observed embedded in the matrix within which they had formed. The results of crucible and prill compositions are presented in Tables 1 and 2.

Multiple spot, areas and bulk assessments of the prills embedded within the three layers of the crucible profile, as well as of the prills isolated from the base of the lid, FAS and crucible slag, were recorded. Analyses of large prill were preferred to smaller prill analyses and if smaller prill analyses were necessary, a spot spectrum was acquired at higher magnifications to avoid capturing data from the background matrix. Those

Table 1. Lists the normalized bulk prill composition in wt.% all elements. The prill composition reported in this table demonstrates the heterogeneity within the prills formed in different crucible matrices. Prills with lower phosphorus bulk concentration can show higher levels of phosphorus in spot analyses given the segregation tendency of phosphorus in steel.

Crucible body (wt.% oxide)	**Na_2O**	**MgO**	**Al_2O_3**	**SiO_2**	**P_2O_5**	**K_2O**	**CaO**	**TiO_2**	**MnO**	**FeO**	**Cru wall size**
Ind-Ibh'19-Cru003 (10)	0.6	1.5	24.2	62.6	0.3	3.3	1.5	0.7	0.1	5.2	(>= 1 cm)
Ind-Chn'19-Cru001D (3)	0.9	2.2	24.5	57.1	0.6	2.0	2.1	1	0.1	9.4	(<= 1 cm)
Ind-Gur'19-Cru001B (8)	0.4	1.7	24.4	61.5	0.1	2.9	1.8	1.2	0.1	6	(<= 1 cm)
Ind-Kp'19-Cru001D (5)	0.8	1.0	24.6	62.7	0.1	5.2	1.6	0.8	0.1	3.2	(>= 1 cm)
Ind-Kp'19-Cru001C (14)	0.8	1.4	25.3	63.5	0.1	3.7	1.2	0.7	0.1	3.1	(>= 1 cm)
Ind-Kp'19-Cru003 base (13)	0.7	1.1	26	62.4	0.2	3.7	1.4	0.6	0.1	3.7	(>= 1 cm)
Ind-Ksm'19-Cru003 (12)	1.1	1.0	22.7	63	0.1	6.1	1.6	0.6	0.1	3.5	(>= 1 cm)
FAG (wt.% oxide)	**Na_2O**	**MgO**	**Al_2O_3**	**SiO_2**	**P_2O_5**	**K_2O**	**CaO**	**TiO_2**	**MnO**	**FeO**	**Cru wall size**
Ind-Ibh-Cru003	1.0	2.8	19.5	55.7	1.4	5.5	7.0	0.7	0.1	6.3	(>= 1 cm)
Ind-Chn'19-Cru001D FAG (13)	1.2	2.2	19.3	65.4	0.2	2.2	3.0	1.2	0.1	5.3	(<= 1 cm)
Ind-Gur'19-Cru001B FAG (6)	0.2	3.5	14.4	58.5	0.1	2.7	17.6	0.6	0.1	2.4	(<= 1 cm)
Ind-Kp'19-Cru001 A (8) FAG fragment	0.9	1.2	22.9	59.3	0.2	5.8	3.1	0.8	n.d.	5.6	(>= 1 cm)
Ind-Kp'19-Cru001D (6) FAG	0.6	3.5	16.5	50.9	0.6	3.7	19.0	0.6	0.1	4.4	(>= 1 cm)
Ind-Ksm'19-Sl002A and B (29) FAS	0.5	5.0	15.3	51.2	1.0	5.3	20.0	0.5	0.1	1.0	
Ind-Ksm'19-Sl002 (20) FAS	0.3	3.7	15.0	46.6	1.7	2.9	27.6	0.6	0.1	1.4	
Crucible slag/crucible slag film (wt.% oxide)	**Na_2O**	**MgO**	**Al_2O_3**	**SiO_2**	**P_2O_5**	**K_2O**	**CaO**	**TiO_2**	**MnO**	**FeO**	
Ind-Ibh'19-Cru003 (9) c.slag film	0.6	2.8	11.5	66.3	n.d.	3.7	11.6	0.8	0.1	4.3	
Ind-Ksm'19-Cru007B (12) c.slag film	0.9	0.5	21.0	65.7	n.d.	6.7	1.0	0.6	n.d.	3.6	
Ind-Ksm'19A-Cru009A (7) c.slag film	0.5	2.5	26.1	51.3	n.d.	2.9	12.1	2.7	0.4	1.5	
Ind-Ksm'19-Sl002D (18) 2 samples c.slag	0.4	3.8	19.3	49.1	<0.2	2.6	21.5	1.7	0.4	1.0	
Ind-Ksm'22-Cru slag a (21) 2 samples c.slag	0.4	4.6	16.7	51.3	n.d.	4.0	20.2	1.1	0.2	1.1	
Ind-Kp'19-Sl007 (12) 2 samples c.slag	0.4	4.1	17.4	51.5	0.1	3.2	20.6	1.6	0.1	3.8	

analyses where the surrounding matrix was included in the spectrum, as indicated by aluminium peaks, were discarded. Variations in alloy compositions inside the bigger prills were identified by collecting, whenever it was practical, several spot and area spectra. The quantification of carbon in the metal proved difficult due to the low accuracy of EDS in determining lighter elements and the need to carbon-coat samples to prevent charging during imaging and analysis. Therefore, the microstructure of the prills as seen in Back-Scatter Electron (BSE) imaging was used as a guide to its carbon concentration. Identification and photographing of any possible microstructures in prills became easier using a high contrast BSE setting.

The compositions of the melt and ceramic bodies surrounding the prills are presented in wt.% oxide with oxygen determined by stoichiometry, while the prill compositions are reported in wt.% as measured for all elements, including oxygen if present. All results have been normalised to 100 weight percent. During analyses, the working distance was kept at 8.50 mm, the EHT at 20 kV, the aperture size at 30 mm and the beam current at 2.5 nA. The beam intensity, stability and channel alignment of the detector were monitored through regular measurements of a copper tape and the analytical total / beam intensity was further monitored by analysing quartz crystals as stoichiometrically pure SiO_2 contained inside the FAG layer of the crucible.

For Merv, sample preparation and SEM-EDS analyses were conducted on newly prepared cross-sections of Merv samples already published by Feuerbach (2002). Identical preparation and analytical techniques and pa-

Table 2. Showing the normalised compositions of FAG/S, crucible body and crucible slag, in wt.%. Compared to the ceramic bodies, the FAG/S region is characterised by high CaO and low alumina concentration, likely due to the contribution from lime-rich fuel ash. Of the other typical FA oxides, potash potentially evaporated due to high operating temperature (Misra, Ragland and Baker, 1993) and phosphate reduced to iron phosphide. Magnesia is elevated as expected. Silica remains similar, indicating silica content in FA. The other FA oxide potash is more or less in varying concentrations (ranging from 1.5-5.8 wt.% oxide) and not significantly enriched in FAG/S. The crucible slag or crucible slag film has an alumina content in the range of 17.4-21 wt.% and high CaO content, except in one instance (Ind-Ksm'19-Cru007B) where the low CaO is compensated by high potash content.

Sample name, matrix, prill no.										
Crucible body prills (wt.% all elements)	**O**	**Al**	**Si**	**P**	**V**	**Cr**	**Fe**	**Ni**	**Cu**	**Others**
Ind-Ibh-Cru 003_prill 18	1.3	0.2	13.5	3.3	n.d.	0.1	81.0	0.1	n.d.	Mn=0.4
Ind-Ibh-Cru 003_prill 3	n.d.	0.2	21.1	1.8	0.1	0.1	75.8	n.d.	n.d.	Ti=0.4, Mn=0.4
Ind-Chn-Cru001 D_prill 11	2.5	0.1	5.7	0.8	0.2	0.2	89.9	0.2	0.1	
Ind-Gur'19-Cru001B_prill 6	n.d.	0.2	16.5	1.5	n.d.	n.d.	81.1	n.d.	n.d.	
Ind-Kp'19-Cru001C_prill 13	2.5	0.2	0.2	13.9	n.d.	n.d.	82.8	0.3	0.1	
Ind-Kp'19-Cru001D_prill 15	0.6	0.2	6.2	0.2	n.d.	n.d.	92.7	0.2	n.d.	
Ind-Kp'19-Cru003 base_prill 5	1.6	0.2	9.1	11.0	0.4	0.2	76.6	0.1	0.2	Ti=0.4, Mn=0.3
Ind-Kp'19-Cru003 base_prill 6	1.7	0.2	11.9	6.5	0.3	0.2	78.4	0.2	0.1	Ti=0.2, Mn=0.3
Ind-Ksm'19-Cru009A_prill 4	n.d.	0.2	1.4	11.9	0.1	n.d.	86.0	n.d.	0.1	
Ind-Ksm'19-Cru009A_prill 5	n.d.	0.2	17.5	2.2	0.1	0.1	79.4	n.d.	0.2	
FAG prills (wt.% all elements)	**O**	**Al**	**Si**	**P**	**V**	**Cr**	**Fe**	**Ni**	**Cu**	
Ind-Chn'19-Cru001 D_prill 2	n.d.	0.2	0.8	0.1	n.d.	n.d.	98.9	n.d.	n.d.	
Ind-Kp'19-Cru001A_prill 11	n.d.	0.1	0.5	2.5	0.2	0.1	96.3	0.1	n.d.	
Ind-Kp'19-Cru001D_prill 2	2.4	0.1	0.2	6.6	n.d.	n.d.	89.8	0.2	n.d.	
Ind-Kp'19-Cru001D_prill 7	2.4	0.2	0.2	2.0	n.d.	n.d.	96.1	0.5	0.1	S=0.3
Ind-Ibh-Cru 003_prill 29	n.d.	0.2	0.4	13.9	n.d.	n.d.	84.9	0.2	0.1	
Ind-Ksm'19-Sl002A_prill 18	n.d.	0.2	0.2	21.1	n.d.	0.1	78.4	n.d.	n.d.	
Ind-Ksm'19-Sl002A_prill 1	n.d.	0.2	0.2	21.0	n.d.	n.d.	78.5	n.d.	0.1	
Ind-Ksm'19-Sl002C_prill 1	n.d.	0.2	0.1	8.3	n.d.	n.d.	91.7	n.d.	0.1	
Ind-Ksm'19-Sl002 slag_large prill	n.d.	0.1	0.1	12.5	n.d.	n.d.	86.1	0.2	0.1	
C.slag (wt.% all elements)	**O**	**Al**	**Si**	**P**	**V**	**Cr**	**Fe**	**Ni**	**Cu**	
Ind-Ibh'19-Cru003 (9)	n.d.	0.2	0.2	0.6	n.d.	n.d.	98.4	n.d.	n.d.	
Ind-Ksm'19-Cru007B_melt 5	0.6	0.2	0.2	0.2	n.d.	n.d.	98.9	n.d.	n.d.	
Ind-Ksm'19-Cru009A_prill 11	n.d.	0.2	0.1	0.6	0.1	0.1	98.5	n.d.	0.1	
Ind-Ksm'19-Sl002D_prill 6	0.6	0.2	0.2	0.1	n.d.	n.d.	98.9	n.d.	n.d.	
Ind-Ksm'22-Cru slag a_prill 1	1.1	0.2	0.1	10.7	n.d.	n.d.	87.7	0.1	n.d.	
Ind-Ksm'22-Cru slag a_prill 2	1.3	0.2	0.1	0.4	n.d.	n.d.	97.7	n.d.	n.d.	S=0.2
Ind-Kp'19-Sl007_prill 12	n.d.	0.2	0.2	12.5	n.d.	n.d.	86.9	n.d.	n.d.	
Ind-Kp'19-Sl007_prill 9	n.d.	0.1	0.5	0.4	n.d.	n.d.	98.8	n.d.	n.d.	

rameters were used for Merv and Telangana samples. The Merv results are analyses of three crucible fragments from bag MGK 4, a big crucible (see Feuerbach, 2002, p.47), which was cross-sectioned along with its base pad ceramic with base pad ceramic glaze, two shiny slag fragments randomly selected from bag Mgu 95 4-47-60 7mm RS (fragment 1 with some crucible body) and crucible slags 3B (with some crucible body attached) and 4B from bag MGK 93. The big crucible and MGK 4 crucible fragments have a thin layer of crucible slag film attached to the body. The Merv sample nomenclature is carried forward from Feuerbach (2002) to avoid confusion and promote reproducibility.

The Merv base pads are a feature added to the crucibles to keep them stable on the furnace floor. The base pad ceramic has a black FAG, which is compositionally similar to the ceramic FAG. The base pad ceramic also appears to have the same composition as the crucible body, although this was not further explored for this study.

Table 3. Composition of Merv crucible body, FAG, crucible slag and base pad ceramic reported in wt.% oxide. A small fragment of crucible body was attached with c. slag3B (frag 1). The fragments are independent samples with same sample labels as curated by Feuerbach (2002). Both the fragments of crucible slag Mgu 95 are high MnO c. slags, analytically identical and likely from the same crucible.

Crucible body (wt.% oxide)	**Na_2O**	**MgO**	**Al_2O_3**	**SiO_2**	**P_2O_5**	**SO_2**	**K_2O**	**CaO**	**TiO_2**	**MnO**	**FeO**	**Sb_2O_3**
3B with some c.body attached	0.4	0.4	29.1	63.5	n.d.	n.d.	4.1	0.7	0.5	0.2	1.1	n.d.
Big crucible	0.2	0.5	29.3	62.9	n.d.	n.d.	3.8	1.2	0.6	0.6	1.0	0.1
MgK 4 (2 frag)	0.3	0.5	28.5	65.0	n.d.	n.d.	3.0	0.6	0.6	n.d.	1.2	0.1
FAG (wt.% oxide)	**Na_2O**	**MgO**	**Al_2O_3**	**SiO_2**	**P_2O_5**	**SO_2**	**K_2O**	**CaO**	**TiO_2**	**MnO**	**FeO**	**Sb_2O_3**
Big crucible FAG	0.3	2.5	24.8	58.6	n.d.	n.d.	2.9	8.7	0.6	0.3	1.3	n.d.
MgK 4 (2 frag) FAG	0.8	2.3	23.8	54.3	0.2	0.6	4.1	12.1	0.5	n.d.	1.0	n.d.
Crucible slag (wt.% oxide)	**Na_2O**	**MgO**	**Al_2O_3**	**SiO_2**	**P_2O_5**	**SO_2**	**K_2O**	**CaO**	**TiO_2**	**MnO**	**FeO**	**Sb_2O_3**
3B	0.4	2.2	20.8	55.6	n.d.	n.d.	2.9	10.6	0.5	4.2	2.6	0.1
4B	0.3	3.4	18.5	52	n.d.	n.d.	2.9	15	0.5	5.2	1.9	0.1
Mgu 95 (2 frag)	0.2	2.5	15.8	47.3	n.d.	0.1	1.4	15.7	0.5	14.7	1.7	0.1
Big crucible (c.slag film)	0.4	1.8	26.4	56.1	n.d.	n.d.	4.4	6.7	0.5	1.9	1.7	0.1
MgK 4 (2 frag) (c.slag film)	0.8	4.1	19.0	52.5	0.6	0.6	2.3	17.3	0.6	0.7	1.6	0.1
Base pad (wt.% oxide)	**Na_2O**	**MgO**	**Al_2O_3**	**SiO_2**	**P_2O_5**	**SO_2**	**K_2O**	**CaO**	**TiO_2**	**MnO**	**FeO**	**Sb_2O_3**
Base pad glaze	0.3	3.0	20.8	53.8	1.0	0.5	2.8	15.7	0.5	0.1	1.4	0.1
Base pad ceramic	0.3	0.7	24.7	65.7	0.1	0.1	3.7	2.6	0.6	n.d.	1.4	n.d.

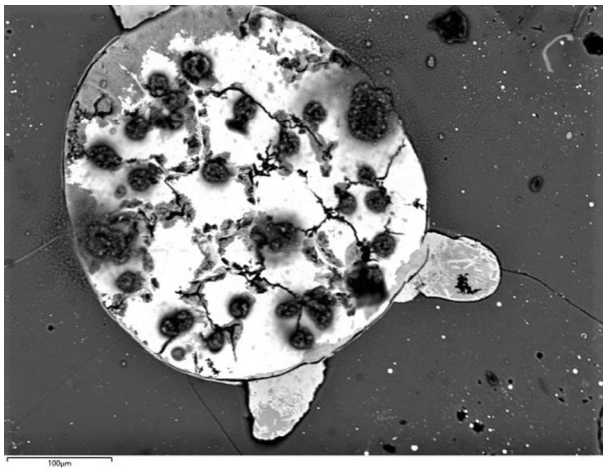

Figure 6. SEM-BSE image of a prill (#7) from crucible lid of Ind-Ksm-Cru003 illustrating graphite formation as nodules and flakes. Silicon ranges from 5.8-8.3 wt.% with very little phosphorus (below detection limit). The graphite formation indicates slow cooling of the prill and is triggered by the high silicon content. Scale: 100 µm or 200 x. Photo: M. Desai and Th. Rehren, Archaeological Science Laboratories, The Cyprus Institute.

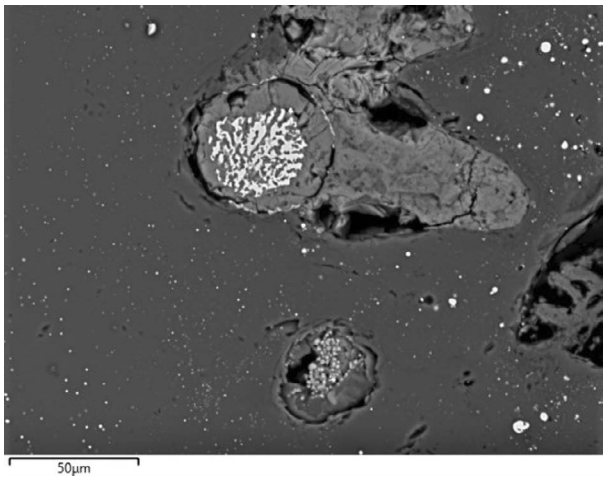

Figure 7. SEM-BSE image of partly corroded prill # 28 formed in a temper cavity in Ind-Ibh'19-Cru003. Corrosion products surround the prill and fill in porosities. In spot analyses, silicon composition in the prill ranges from 15-17 wt.% and phosphorus from 0.3-1.6 wt.%. Scale: 50 µm or 500 x. Photo: M. Desai and Th. Rehren, Archaeological Science Laboratories, The Cyprus Institute.

Tables 3 and 4 give the most typical composition values of Merv crucibles, crucible slag, base pad ceramic and prills. Given the enormous compositional variance that can exist between any two prills, using the average weight percentage of all collective prills in a single crucible profile would be misleading. For the Telangana samples, the crucibles and slags are labelled with their country code (Ind), site code (Kp/Gur/Ksm etc.), year of collection and sample type (crucible [cru]/slag [sl]) and a running number; details of these samples will be published separately (forthcoming Desai, 2023). Each prill number corresponds to a unique prill in the individual sample.

Table 4. Normalised composition of Merv prills reported in wt.% all elements formed within the crucible body, glaze, slag and base pad ceramic. Please note, fragment 1 of Mgu 95 crucible slags and crucible slag 3b have some crucible body attached.

Sample name, matrix, prill no.																			
Crucible body (wt.% all elements)	**O**	**Na**	**Mg**	**Al**	**Si**	**P**	**S**	**K**	**Ca**	**Ti**	**V**	**Cr**	**Mn**	**Fe**	**Ni**	**Cu**	**As**	**Sn**	**Sb**
MgK 4 c.body prill 1	0.9	n.d.	n.d.	0.2	0.1	1.1	0.6	n.d.	n.d.	n.d.	n.d.	n.d.	0.1	91.8	2.3	0.4	1.9	0.4	0.2
Mgk 4 c.body prill 2	3.9	n.d.	n.d.	1.2	1	7.2	0.7	0.1	0.1	0.1	n.d.	n.d.	n.d.	78.9	5.7	0.5	n.d.	0.3	n.d.
MgU 95 c.body prill quartz periphery	3.0	n.d.	0.1	0.4	5.9	0.6	n.d.	0.2	n.d.	n.d.	0.1	n.d.	0.2	88.5	0.3	0.3	n.d.	0.5	n.d.
Big crucible c. body prill 1	5.4	n.d.	0.1	1.6	1.7	4.3	0.2	0.2	0.1	0.1	n.d.	n.d.	n.d.	84.5	1.6	0.1	0.1	n.d.	n.d.
Big crucible c.body prill 2	0.7	n.d.	n.d.	0.2	0.2	0.5	n.d.	0.1	n.d.	n.d.	n.d.	n.d.	0.1	97.3	0.2	0.2	0.4	n.d.	n.d.
Body attached C.slag 3B prill 1	2.5	n.d.	n.d.	0.3	0.3	15.2	0.1	0.1	n.d.	n.d.	n.d.	n.d.	n.d.	78.5	2.1	0.1	0.6	n.d.	n.d.
FAG (wt.% all elements)	**O**	**Na**	**Mg**	**Al**	**Si**	**P**	**S**	**K**	**Ca**	**Ti**	**V**	**Cr**	**Mn**	**Fe**	**Ni**	**Cu**	**As**	**Sn**	**Sb**
MgK 4 FAG prill 1	6.0	0.5	0.5	1.0	7.3	4.3	0.1	0.3	1.0	0.2	0.1	0.1	0.2	78.3	0.1	0.2	n.d.	n.d.	n.d.
Big crucible FAG prill 1	2.2	n.d.	0.1	0.5	0.8	7.7	0.1	0.1	0.2	n.d.	n.d.	n.d.	0.1	83.5	4.4	0.2	0.1	0.1	n.d.
FA glaze Fe-prill 6 aa 1	6.2	0.8	0.6	0.3	2.6	10.4	0.3	0.1	0.9	0.1	0.2	0.2	0.1	75.2	1.1	0.2	0.4	0.1	0.2
Crucible slag/crucible slag film (wt.% all elements)	**O**	**Na**	**Mg**	**Al**	**Si**	**P**	**S**	**K**	**Ca**	**Ti**	**V**	**Cr**	**Mn**	**Fe**	**Ni**	**Cu**	**As**	**Sn**	**Sb**
MgU 95 prill 5 Frag 1	1.0	n.d.	n.d.	0.2	0.1	0.1	n.d.	n.d.	n.d.	n.d.	n.d.	n.d.	0.3	98.0	n.d.	0.2	n.d.	n.d.	n.d.
MgU 95 prill 9	0.8	n.d.	n.d.	0.1	0.1	0.1	n.d.	n.d.	0.1	n.d.	n.d.	n.d.	0.1	98.3	n.d.	0.3	n.d.	n.d.	n.d.
MgU 95 prill 11 Frag 2	0.8	n.d.	n.d.	0.2	0.1	0.6	n.d.	n.d.	0.2	n.d.	n.d.	n.d.	0.4	97.2	0.1	0.4	n.d.	n.d.	n.d.
C.slag 3B prill 10	0.9	n.d.	n.d.	0.2	0.2	0.3	n.d.	0.1	0.4	n.d.	n.d.	n.d.	0.4	97.5	0.1	0.4	n.d.	n.d.	n.d.
C.slag 4B prill 4	0.9	n.d.	n.d.	0.2	0.1	n.d.	n.d.	n.d.	n.d.	n.d.	n.d.	n.d.	0.2	98.3	0.1	0.1	0.1	n.d.	n.d.
MgK c.slag prill 1	1.8	1.1	0.2	0.2	0.2	0.1	0.1	0.1	0.2	n.d.	n.d.	n.d.	n.d.	95.4	0.1	0.5	n.d.	0.1	0.1
MgU c.slag film prill 1 aa	1.8	1.1	0.2	0.2	0.2	0.1	0.1	0.1	0.2	n.d.	n.d.	n.d.	n.d.	95.4	0.1	0.5	n.d.	0.1	0.1
Vitrified base pad and base pad ceramic prills (wt.% all elements)	**O**	**Na**	**Mg**	**Al**	**Si**	**P**	**S**	**K**	**Ca**	**Ti**	**V**	**Cr**	**Mn**	**Fe**	**Ni**	**Cu**	**As**	**Sn**	**Sb**
vit_base pad_FeS prill aa 1	3.0	n.d.	n.d.	0.1	0.1	0.1	33.0	n.d.	0.1	n.d.	n.d.	0.1	0.3	54.5	0.3	8.1	0.2	n.d.	n.d.
vit_base pad_FeS prill 2	2.7	n.d.	n.d.	0.3	0.6	0.1	36.1	0.1	0.5	n.d.	n.d.	0.2	0.2	58.2	0.3	0.5	0.2	n.d.	n.d.
vit_base pad_FeS prill aa 2	2.0	n.d.	n.d.	0.2	0.1	0.1	34.8	n.d.	0.1	n.d.	n.d.	0.1	0.4	60.4	0.2	1.4	0.1	n.d.	n.d.
Vit ceramic prill 2	6.9	n.d.	n.d.	0.2	0.3	0.2	40.9	0.1	0.4	n.d.	n.d.	0.1	0.1	36.9	1.7	11.5	0.7	n.d.	n.d.

Results

Telangana

Crucibles

The clay used for the Telangana crucibles is high in alumina and medium rich in iron oxide and several percent by weight potash; it is heavily tempered with rice husk. The crucible bodies are black and porous. A mullite crystal network formed across the crucible body, which is a characteristic of alumina rich crucibles fired to high temperature (e.g., Lowe, Merk and Thomas, 1990; Martinón-Torres, Rehren and Freestone, 2006). The FAG and crucible slags here are higher in lime, potash and magnesia and lower in their silica and alumina content as compared to the crucible body.

Prills

We present the prills here according to their associated crucible regions, i.e. first the crucible body prills, then the as FAG/S prills, followed by prills in the crucible slag film/crucible slag; in each case with some comments on their microenvironment within which they have formed (Figures 6 to 19).

The crucible body prills are high in silicon with a significant presence of phosphorus in some prills. Silicon in high-carbon alloys leads to the formation of graphite as needles and nodules at the expense of cementite. Accordingly, graphite-containing high silicon prills are seen in all crucible types, regardless of size. Both silicon and carbon were available in the body matrix, due to the high amount of added organic temper rich in siliceous phytoliths.

Figure 8. High contrast SEM-BSE image of prill #6 from Ind-Gur'19-Cru001B. Area analysis quantifies high silicon (~15 wt.%) and low phosphorus (~3.8 wt.%). The melt forms within temper porosity; both porosity and ceramic matrix are black due to the high contrast setting. The entire cluster of iron melts/prills shows high values of silicon (9-16.6 wt.%) and phosphorus (1.8-8.7 wt.%). Scale: 250 µm or 100 x. Photo: M. Desai and Th. Rehren, Archaeological Science Laboratories, The Cyprus Institute.

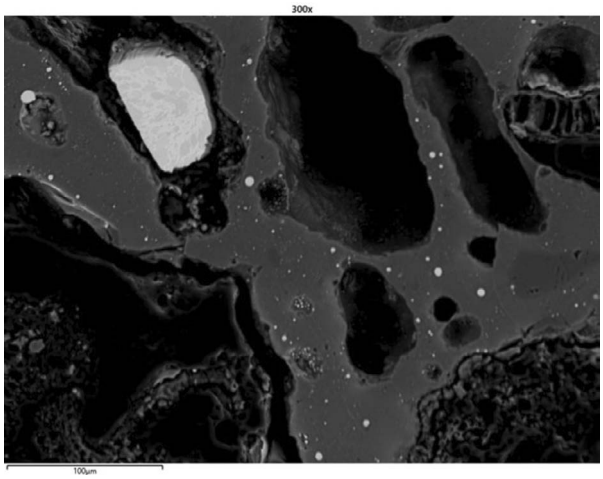

Figure 9. SEM-BSE image of melt # 13 in disintegrated rice husk porosity from Ind-Kp'19-Cru001C. The area analyses show phosphorus in the range of 11.5-13.9 wt.%. Scale: 100 µm or 200 x. Photo: M. Desai and Th. Rehren, Archaeological Science Laboratories, The Cyprus Institute.

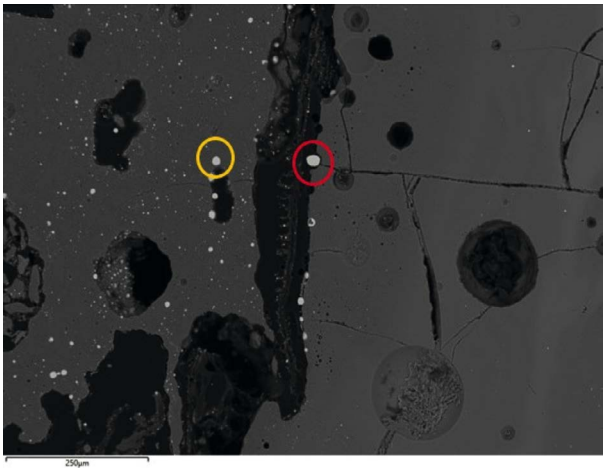

Figure 10. SEM-BSE image of prill #5 (on left in yellow circle) and prill #6 (on right in red circle) formed near disintegrated temper in Ind-Kp'19-Cru003. The prill #5 contains 9 wt.% silicon and 11 wt.% phosphorus and prill #6 contains 11.9 wt.% silicon and 6.5 wt.% phosphorus. Scale: 250 µm or 100 x. Photo: M. Desai and Th. Rehren, Archaeological Science Laboratories, The Cyprus Institute.

Figure 11. High contrast SEM-BSE image of FAG Prill #2 from Ind-Chn'19-Cru001D, characterized by low silicon (0.8 wt.%) and phosphorus (0.1 wt.%) concentrations. The prill has a cementite-pearlite microstructure with inter-granular porosities and beginning corrosion. Scale: 50 µm or 500 x. Photo: M. Desai and Th. Rehren, Archaeological Science Laboratories, The Cyprus Institute.

Telangana FAS and FAG iron prills have a higher concentration of phosphorus than the crucible body, crucible slag film and crucible slag prills, but they rarely contain silicon. Instead, the prills in FAG and FAS quantify phosphorus as high as 20 wt.%. Only in the smaller crucible varieties with a smaller diameter (<=5 cm) and thinner wall size (<=1 cm), where the FAG layer was less distinct, silicon alloyed with iron prills in the FAG region, similar to the crucible body prills nearby.

The prills in the crucible slag film and crucible slag have no silicon and only some phosphorus, but less so than the FAS/FAG prills (Figure 26). While there are systematic differences in prill composition between the different layers, it remains challenging to classify prills based on their origin alone. However, the body

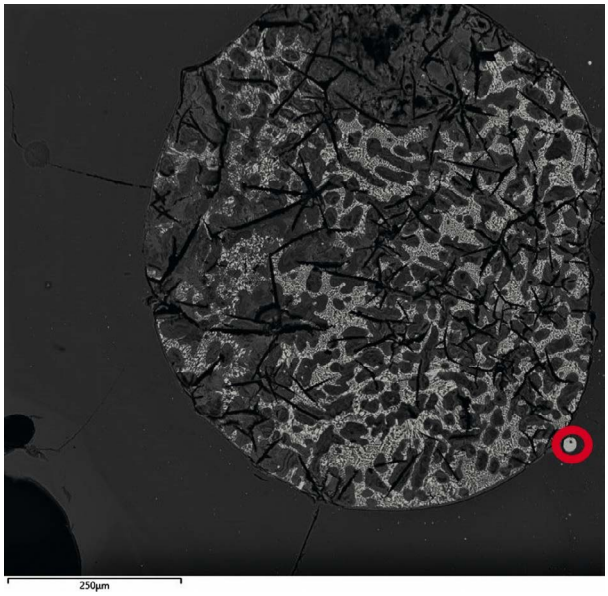

Figure 12. SEM-BSE image of FAG Prill #3 with elongated graphite flakes and corrosion of a dendritic phase, probably austenite / pearlite, from Ind-Gur'19-Cru001. The matrix is a partly-corroded eutectic of iron, phosphorus and silicon, and probably some carbon. The silicon and phosphorus content in the non-corroded region of prill #3 are 2.6 wt.% and 15.8 wt.% respectively. The bulk silicon and phosphorus (including the corrosion) are 16.3 and 16.6 wt.% respectively. The tiny prill #4 sitting on the lower tangent of prill #3 has high silicon (11.6 wt.%) and relatively low phosphorus (3.5 wt.%). Scale: 250 µm or 100 x. Photo: M. Desai and Th. Rehren, Archaeological Science Laboratories, The Cyprus Institute.

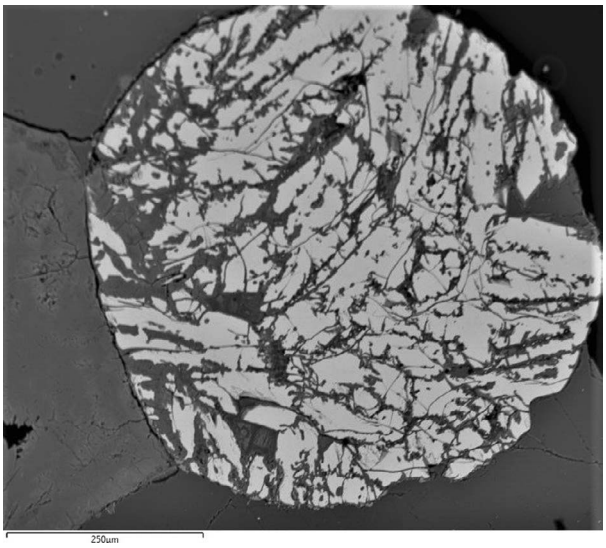

Figure 13. SEM-BSE image of Prill #15 from crucible Ind-Ibh'19-Cru003. This FAG prill contains 1.3-3.8 wt.% silicon and 16-19 wt.% phosphorus. The main metal phase is probably Fe3P. Corrosion primarily seen on the grain boundaries. Scale: 250 µm or 100 x. Photo: M. Desai and Th. Rehren, Archaeological Science Laboratories, The Cyprus Institute.

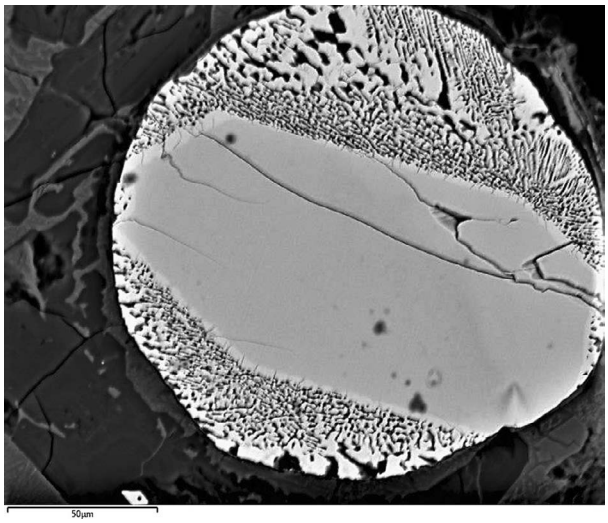

Figure 14. SEM-BSE image of Prill #17 from FAS Ind-Ksm'19-sl002A with 15-21 wt.% phosphorus. Phosphorus is higher in the central medium grey region (21 wt.%, probably the Fe2P phase) as compared to the surrounding Fe-Fe3P eutectic (15 wt.%); we assume that the Fe part of the eutectic is corroded out (now black). No silicon was found above the detection limit. Scale: 50 µm or 500 x. Photo: M. Desai and Th. Rehren, Archaeological Science Laboratories, The Cyprus Institute.

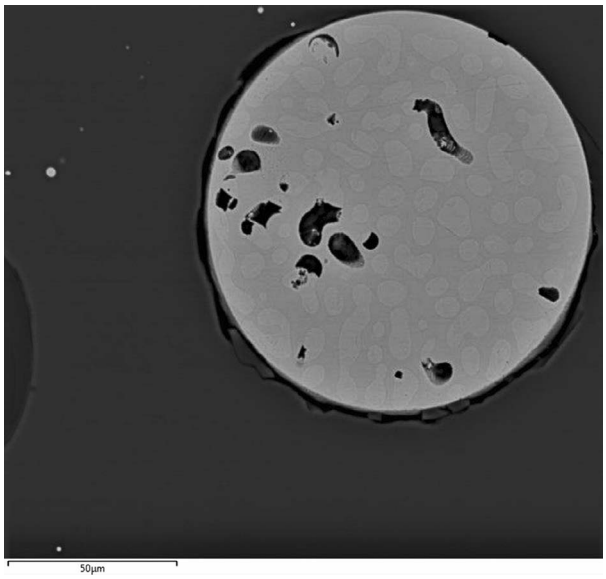

Figure 15. SEM-BSE image of Prill #1 in FAS Ind-ksm'19-sl002C. Pearlite grains in phosphorus-rich matrix, with some corrosion of the pearlite. The light islands show a lower phosphorus (2.4 wt.%) content as compared to the darker background (12.3 wt.%). The preferential corrosion of low phosphorus island is consistent with the anti-corrosive property of phosphorus in steel. Area analyses report overall phosphorus in range of 7-8 wt.%. No silicon was found above the detection limit. Scale: 50 µm or 500 x. Photo: M. Desai and Th. Rehren, Archaeological Science Laboratories, The Cyprus Institute.

Figure 16a. Large prill (1cm diameter) partly embedded in FAS Ind-Ksm'19-sl002. Photo: M. Desai and Th. Rehren, Archaeological Science Laboratories, The Cyprus Institute.

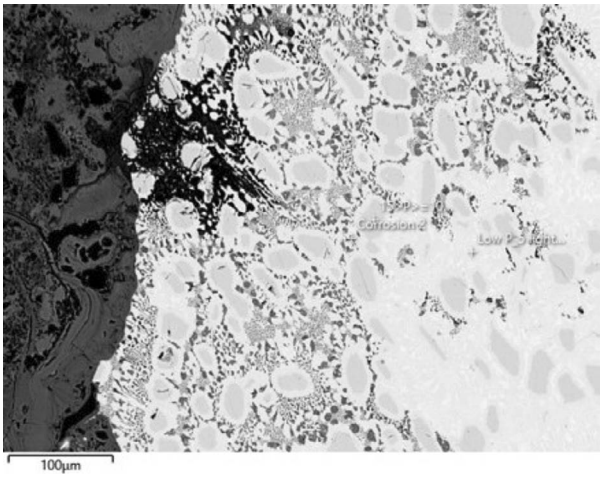

Figure 16b. SEM-BSE image of the prill. The light grey regions have low phosphorus content between 2-5 wt.% and the darker regions have 10-15 wt.% phosphorus. The specimen contains Fe (small bright white phase, preserved only in the right part of the image), Fe3P3 (light grey) and Fe2P2 (darker grey). The Fe-Fe3P eutectic forms the matrix; in the left and central part of the image, Fe is mostly corroded. Compare above, Figure 14, for the same arrangement. Scale: 100 µm or 200 x. Photo: M. Desai and Th. Rehren, Archaeological Science Laboratories, The Cyprus Institute.

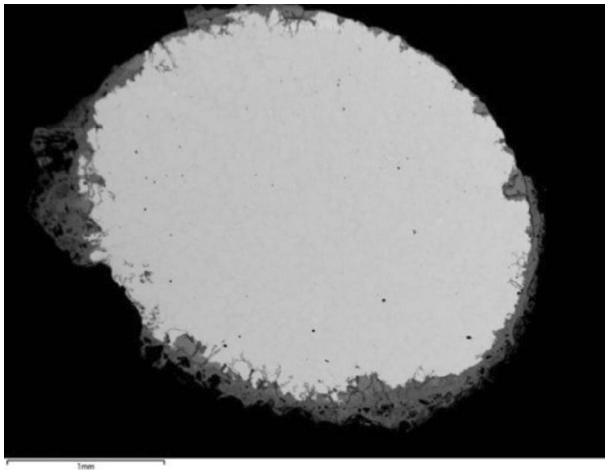

Figure 17a. SEM-BSE image of a large prill isolated from crucible slag Ind-Ksm'19- Sl002D. The corrosion on the outer edge of the prill is progressing along the grain boundaries. The bulk analysis indicates Si = 0.2 wt.% and P = 0.2 wt.%. Scale: 1mm or 30 x. Photo: M. Desai and Th. Rehren, Archaeological Science Laboratories, The Cyprus Institute.

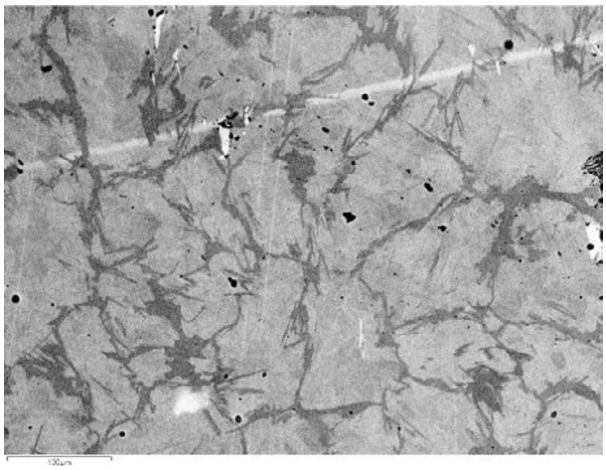

Figure 17b. High-contrast SEM-BSE image of the microstructure of the prill, showing grain boundary cementite in a pearlite matrix along with some shrinkage porosity. The hyper-eutectoid prill composition and microstructure correspond to the analysed ingots from Konasamudram. Scale: 250 µm or 100 x. Photo: M. Desai and Th. Rehren, Archaeological Science Laboratories, The Cyprus Institute.

prills are systematically much higher in silicon, reaching to around 20 wt.% Si, while FAG/FAS prills are more likely to be high in phosphorus, reaching up to around 20 wt.% P but not exceeding 1 wt.% Si (see Table 1). The differences in prill composition do not, therefore, reflect the bulk composition of the micro-environment within which they formed (Table 2), but the specific mineralogy and gas atmosphere at the point of their formation (see below).

Merv results

Crucibles

The kaolinitic clay used for the Merv crucibles is high in alumina and low in iron oxide and tempered with grog and quartz (Feuerbach, 2002, p.49). In comparison to the Telangana crucibles, the Merv crucibles are compact and less porous. Silica and alumina are the major oxides in the crucible body with some potash, around 1 wt.%

Figure 18. High contrast image of prill #8 (crucible slag film) from Ind-Ksm'19-Cru009A. Area analysis shows that the composition is low in phosphorus (0.3 wt.%). The prills shows cementite needles in austenite / pearlite matrix, indicating a high carbon content. Scale: 50 µm or 500 x. Photo: M. Desai and Th. Rehren, Archaeological Science Laboratories, The Cyprus Institute.

Figure 19. High contrast SEM-BSE image of prill #6 from crucible slag Ind-Ksm19-sl002D. The microstructure shows pearlite with cementite lamellae and a phosphorus-rich intergranular matrix. The spot analyses show high P content in the matrix (7.5-8.6 wt.%) demonstrating segregation of phosphorus into the residual melt during austenite formation. The pearlite has about 0.6 wt.% phosphorus. Scale: 50 µm or 500 x. Photo: M. Desai and Th. Rehren, Archaeological Science Laboratories, The Cyprus Institute.

iron oxide and slightly lower lime (Table 3). A mullite crystal network formed across the crucible body, which is a typical characteristic of alumina rich crucibles fired to high temperature (Lowe, Merk and Thomas, 1990; Martinón-Torres, Rehren and Freestone, 2006). FAG and crucible slags are higher in lime and magnesia and lower in their silica and alumina content as compared to the crucible body. The crucible slags also show a prominent lime rich anorthite phase. Some crucible slags contain higher manganese oxide in comparison to the others. Feuerbach (2002, pp.75-77) divided the crucible slag into MnO rich and MnO poor groups based on the MnO concentration in the slag. The crucible slag film has a composition close to the composition of crucible slag. The crucible slag film and crucible slag distinction seem unnecessary. However, in both the crucible slag films i.e. in the big crucible and MGK 4 (in 2nd fragment), the MnO content is lower compared to the crucible slags. The iron oxide concentration is more or less consistent across the crucible profile ranging from 1-2 wt.% oxide.

Prills

The smaller sizes of the Merv prills makes them difficult to analyse and quantification occasionally included signals from the background glassy matrix; accordingly, we omitted any prills with more than 3 wt.% oxygen in the EDS data (Table 4). Few prills were large enough for area analyses, as shown in Figures 20 to 25. The little iron oxide from the crucible clay reduces to prills; however, the prills are minute white spots under the SEM and are not as profound as those seen in Indian, Chāhak (Alipour, 2017) and Kudadabad (Güder, et al., 2022) crucibles.

The FAG prills are enriched in phosphorus (especially in prill #1 in big crucible FAG and prill #6 in MGK 4: see Table 4). All non-ferrous elements in the FAG prills are below or about 1 wt.%. Phosphorus and silicon are prominent in FAG prills, but follow no specific pattern.

The crucible body prills show some phosphorus enrichment. The prills (prill 1_c. slag 3B and prill 1 big crucible) with high phosphorus, usually form within cavities in the ceramic matrix. However, prill 1 from the big crucible has associated oxygen, aluminium, silicon and nickel enrichment. Some body prills contain arsenic, minor quantities of copper, tin and antimony (below the detection limit to 1.8 wt.%). The large prill #1 in MGK 4 fragment 2 and prill 1 in MGK 4 fragment 1, shows a high sulfur concentration (6.5 and 5.2 wt.% respectively). The prills are formed on the edge of the pore/void and the iron sulfide rich phase with around 25-30 wt.% sulfur is segregated on the grain boundary. Sulfur, phosphorus and silicon show prominently in the crucible body prills.

The crucible slag film is an extremely thin layer on the inner wall of the Merv big crucible and MGK 4 crucible (fragment 2). Crucible slag prills show no major alloying element or enrichment. No traces of nickel, tin or antimony are detected, but some copper content persists. Both fragments of crucible slag Mgu 95 have very high MnO concentration fragments (14-15 wt.% oxide) whereas, crucible slags 3B and 4B have moderate MnO (4-5 wt.%) and the two crucible slag films have even lower MnO content (0.5-2 wt.% oxide). The concentration

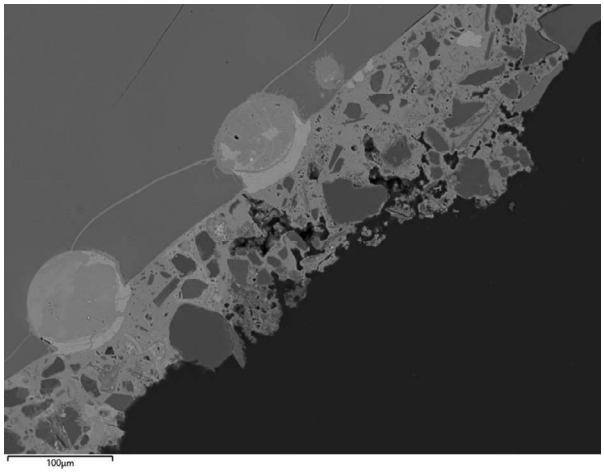

Figure 20. SEM-BSE image of Merv crucible slag (dark grey, upper left) from MgU 95 fragment 1 with corroded prills (light grey). The diagonal band in the middle consists of soil particles (felspar and quartz) trapped in corrosion. Black (lower right) is mounting resin. Scale: 100 µm or 200 x. Photo: M. Desai and Th. Rehren, Archaeological Science Laboratories, The Cyprus Institute.

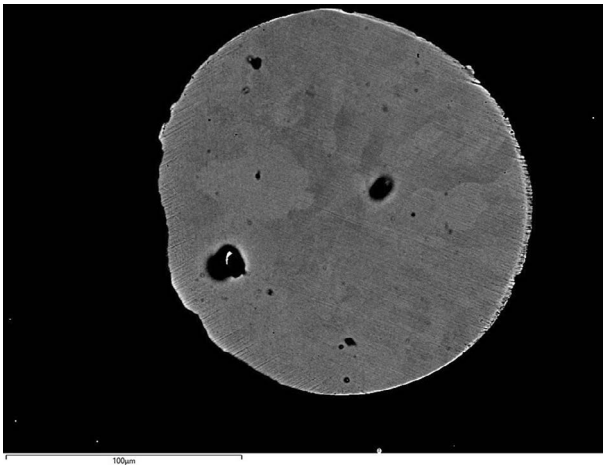

Figure 21. High-contrast SEM-BSE image of Merv crucible slag prill 5 in MgU 95 fragment 2. The prills shows a pure pearlitic microstructure with only trace amounts of nickel and copper. Scale: 100 µm or 200 x. Photo: M. Desai and Th. Rehren, Archaeological Science Laboratories, The Cyprus Institute.

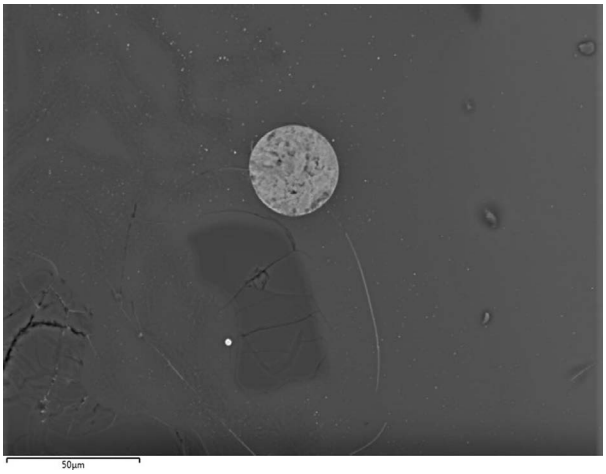

Figure 22. SEM-BSE image of Prill #7 between crucible slag and crucible body in MgU 95. The prill is rich in silicon, likely reduced from excess silica from the quartz grain into the prill. Area analysis gives high silicon (6 wt.%) and low phosphorus (0.6 wt.%), with trace amounts of aluminium (est. 0.4 wt.%), nickel and copper (est. 0.3 wt.% each). Scale: 50 µm or 500 x. Photo: M. Desai and Th. Rehren, Archaeological Science Laboratories, The Cyprus Institute.

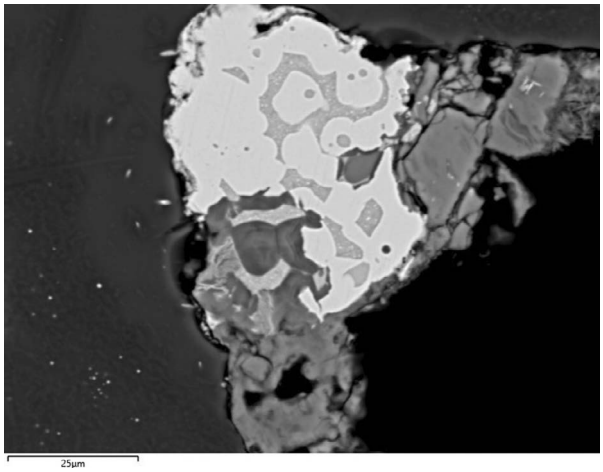

Figure 23. SEM-BSE image of crucible body prill #1 from MgK 4 (frag 1), with enrichment of sulfur (bulk 0.6 wt.%), some phosphorus (0.2-1.1 wt.%), nickel (1-2.3 wt.%) and arsenic (1.9 wt.%); the balance is iron. Scale: 25 µm or 1 Kx. Photo: M. Desai and Th. Rehren, Archaeological Science Laboratories, The Cyprus Institute.

of MnO in crucible slag showed no significant change in Mn content in the crucible slag prills.

The Merv base pad (of the big crucible) prills are very high in sulfur (30-40 wt.% nearly one-third of the normalised values) with significant copper (0.5-11.5 wt.%) (see Table 4). Some corrosion is observed in these prills. There is no reason to assume that any of the crucibles of our Merv analyses were used for any other metal than crucible steel; thus, it is highly unlikely that the non-ferrous prills in the base pad come from the charge of a cracked crucible.

Discussion

The results have shown that iron-rich prills are widespread across all three zones of the crucible profiles, but with varying alloy compositions. We assume that all prills contain significant carbon content, up to as much as 2 to 3 wt.%; unfortunately, our analytical methods did not allow for a quantification of the carbon content. Larger prills showed a microstructure typical of high-carbon steels (see, e.g., Figures 17b, 18 and 19); however, smaller prills did not. Here, it is the fact that

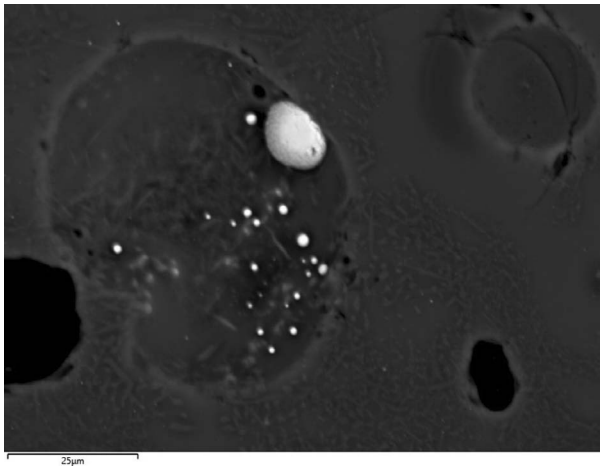

Figure 24. SEM-BSE image of a cluster of prills in a cavity in crucible body attached to Merv c. slag 3B. Prill #1 is the largest prill with 15-16 wt.% phosphorus, while the smaller prills show varying phosphorus content. Scale: 25 µm or 1 Kx. Photo: M. Desai and Th. Rehren, Archaeological Science Laboratories, The Cyprus Institute.

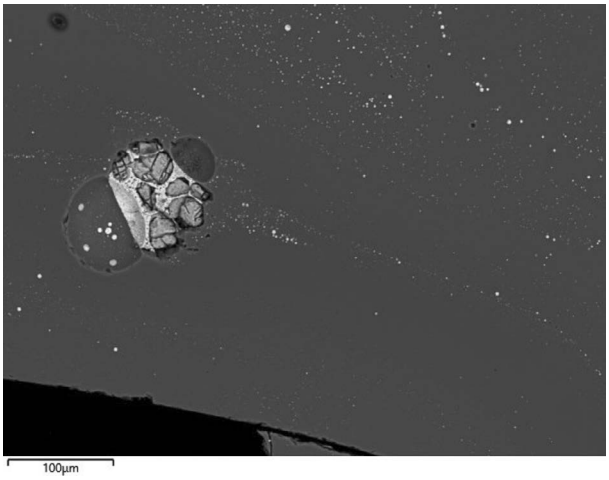

Figure 25. SEM-BSE image of partly corroded iron-sulfur prill #9 in base pad glaze from the big crucible. Scale: 100 µm or 200 x. Photo: M. Desai and Th. Rehren, Archaeological Science Laboratories, The Cyprus Institute.

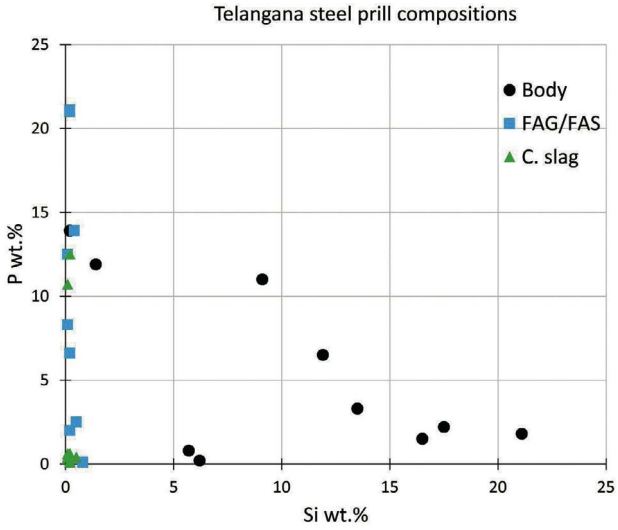

Figure 26. Plot of silicon vs phosphorus concentrations in prills across Telangana crucible profiles from Table 2. Most FAG/S prills and some C.slag prills show a lower silicon and higher phosphorus concentration in comparison to C.body prills. C.body prills typically have a higher silicon concentration but may contain significant quantities of phosphorus as well. Illustration: M. Desai and Th. Rehren, Archaeological Science Laboratories, The Cyprus Institute.

they were evidently liquid at the time of their formation, as indicated by their roundness, which indicates a sufficiently high carbon content to facilitate their melting at the operating temperature. Furthermore, the overall very carbon-rich highly reducing environment in which they formed makes a significant carbon content in the prills highly likely.

Telangana – iron-rich ceramics

Regardless of the size and thickness of the investigated crucibles, the two main alloying elements in Telangana iron prills beyond carbon are silicon and phosphorus. The crucibles with wall thickness >=1cm have a well-developed profile of inner slag, crucible body and outer FAG. In these cases, crucible body prills are very variable in composition, but often high in silicon and / or phosphorus (silicon mostly outweighing phosphorus). FAS/FAG prills are predominantly alloyed with phosphorus at even higher levels than in the body prills, but rarely contain silicon, while the crucible slag/slag film prills may or may not be alloyed with phosphorus (Figure 26). In contrast, in thin-walled crucibles, silicon is also found in FAG prills, as well as in crucible body prills. Thus, the thin-walled crucible shows only a subtle difference in composition between the body and the FAG (Figure 27). Further work is needed to determine whether this is a unique feature of this particular crucible, or a more systematic pattern.

Sources of phosphorus in iron prills

There are several possible sources for phosphorus to enter the iron prills in highly reducing environments. First, phosphoric iron may have been used as feedstock for the process, based on phosphorus-rich ore (Vega, et al., 2003; Godfrey, 2007; Thiele, Török and Költo, 2012). Beyond this, there are several further sources of phosphorus to be considered.

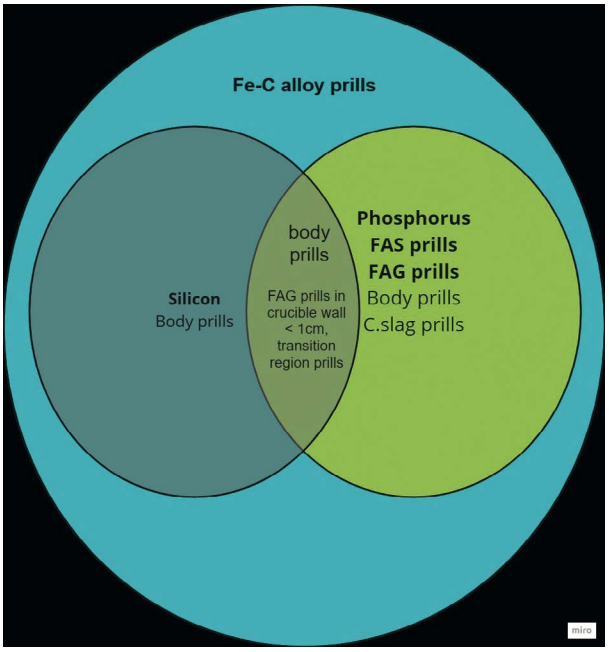

Figure 27. Schematic of alloying patterns in the prills formed in Telangana crucibles. All prills are assumed to contain carbon; additionally, silicon is present mostly in body prills, while phosphorous can be present in all prills, but occurs predominantly in FAG / FAS prills. Illustration: M. Desai and Th. Rehren, Archaeological Science Laboratories, The Cyprus Institute.

a) Apatite

Apatite is probably the most likely source of phosphorus in iron prills in the crucible body. Apatite could be naturally present in the clay used to make the crucibles or as a contaminant of the sand used as a temper. SEM-EDS bulk analyses of the Telangana ceramic bodies indicate overall P_2O_5 contents in the order of 0.1 to 0.6 wt.%. Not only would the total amount of apatite in the body material be sufficient to explain the phosphorus content in the prills across the crucible profile, but the localised nature of discrete apatite grains would also explain the highly variable concentrations of P in these prills.

The situation is different for the prills in the crucible slag. For Chāhak, the addition of apatite as part of the additives in the crucible charge has been proposed as the source of phosphorus in the resulting steel ingot (Alipour and Rehren, 2023) and this is likely reflected in the composition of the small prills trapped in the crucible slag from that site. Whether this specific addition can be assumed for any other production site is currently unknown. For Telangana, no such mineral additives to the crucible charge are known or suspected. However, the crucible slag contains relatively high values of lime, given the limited availability of wood and resulting wood ash in the charge within the crucible cannot enrich the lime sufficiently in the crucible slag. This leaves the possibility of additional lime coming from the bloomery iron slag trapped in the feedstock, or the addition of an as yet unknown other lime rich source added as a flux into the crucible.

b) Fuel ash phosphates:

Fuel ash, is a major source of phosphorus, especially in the FAG/S prills. Wood and other organic fuels are known to contain various amounts of phosphate (Godfrey, 2007, p.48, 60) in addition to the other ash components, primarily lime and silica (Reinmöller, et al., 2021). According to the oral histories of smelters recorded by the Pioneering Metallurgy project (2011) and discussed by Neogi (2017, p.121), teak and *Acacia Catechu* wood, locally known as Sandra, dominates the Northern Telangana forest flora, and are exploited for iron smelting. Assuming the same source of charcoal has been used as fuel for crucible steel production, we can calculate the elemental contributions of wood ash using published data.

The enriched lime content of the FAG and FAS compared to the ceramic body can be explained through fuel ash interaction. The wood ash data (Table 5) indicates a P_2O_5 to CaO ratio of 1:6; in FAG lime values average 8.5 wt.%, while phosphate values are between 0.1-1.4 wt.%, averaging 0.5 wt.% and a ratio of 1:17. Thus, the fuel ash provides a multiple of the phosphate actually contained in the FAG incl. the prills, indicating that some phosphate is either volatilised, or removed as elemental phosphorus alloyed into larger iron prills that separate from the FAS (see Figure 16b).

c) Rice husk as a source of phosphorus in crucible body prills

In addition to the assumed dominant role of apatite as a phosphorus source in most body prills, there is a possibility that the rice husk used as temper in some crucibles may have contributed some phosphorus. However, the available data on the rice husk composition (Mehta,

Table 5. Teak wood ash data from torrefied teak wood from Nigeria, Africa. Indian teak wood will vary in compositions based on the difference in soil and climate. Total ash content of 2 % for wood dried at 320 °C; adapted from Adeleke, et al. (2020).

Oxides in wt.%	SiO_2	Al_2O_3	TiO_2	FeO	CaO	MgO	Na_2O	K_2O	SO_3	P_2O_5
Teak ash	30.3	4.9	0.3	3.2	26.8	5.4	3.0	18.3	3.2	4.2

1992; Ikpo and Okpala, 1992; Zhang and Malhotra, 1996; Bui, Hu and Stroeven, 2005; Ganesan, et al., 2008; Memon, Shaik and Akbar, 2011; Chopra and Siddique, 2015; Kannan and Ganesan, 2016) shows phosphate in rice husk as a minor constituent. However, phosphate values are higher in the Nigerian rice husk (Raheem and Kareem, 2017). Therefore, if the phosphates are present in the local rice husk variety, it could contribute to phosphorus enrichment in the body prills.

The source of silicon in the prills

The presence of silicon in Telangana crucibles is restricted to body prills, which have an average of 10 wt.% Si and reaching 20 wt.% in the extreme. Rostoker and Bronson (1990, p.107-108) discuss in detail the reduction of silicon into iron, as observed mostly in blast furnace operations; here, we see a similar phenomenon but under different process conditions. Notably, these prills seem to be associated with burnt-out organic temper (e.g. Figures 6-12), typically elongated porosity resembling the rice husk structure (Balasubramaniam, Pandey and Jaikishan, 2007; Freestone and Tite, 1986). No dumbbell shaped phytoliths are observed in the crucibles that could point to adding rice straw as temper (Athira, Bahurudeen and Appari, 2021). In contrast, Telangana FAG and crucible slag prills show on average less than 0.4 wt.% silicon, with individual prills not exceeding 1 wt.% Si. Since the temperature and redox conditions between the three different layers were identical, it is apparent that the different chemical environment resulted in the different compositions. Dry rice husk contains about 75 % of organic matter and about 25 % ash (Raheem and Kareem, 2017) and the vast majority of this ash is silica, ranging from 75 to 90 wt.%, with only phosphate and alumina exceeding 5 wt.% in some analyses (Mehta, 1992; Ikpo and Okpala, 1992; Zhang and Malhotra, 1996; Bui, Hu, and Stroeven, 2005; Ganesan, Rajagopal, and Thangavel 2008; Memon, Shaikh, and Akbar, 2011; Chopra and Siddique, 2015; Kannan and Ganesan, 2016; Singh, 2018; Siddika, et al., 2021).

In the Telangana body prills, the silica from the rice husk is exposed to highly reducing conditions, apparently sufficient to convert it to elemental silicon. This reaction reflects the microenvironment around the prills, with the carbon from the temper itself accelerating the reduction. However, according to the Ellingham Diagram (see Figure 3), even at temperatures around 1400 °C silica should not be reduced to silicon by carbon alone, since the Si + O_2 = SiO_2 equilibrium falls below the C + O_2 = CO_2 line. We argue that it is close enough to facilitate some partial reduction of SiO_2 to Si, similar to the evaporation of water even below the boiling point. Rather than re-oxidising in accordance to the equilibrium reaction, some of this silicon then is likely absorbed by a neighbouring iron prill acting as a sink, thus being removed from the system and maintaining a constant reduction to silicon, even though the formal equilibrium requirements for silicon reduction of the Ellingham Diagram are not met. Thus, this formation of silicon-rich iron prills is conditional on the presence of pure silica particles with a large reactive surface, high temperature, strong reducing gas atmosphere and a nearby iron prill collecting the silicon as it forms: A situation uniquely present in the rice-husk tempered iron-rich ceramics of Telangana. Since most of these silicon-phosphorus body prills form on the edge of the disintegrated rice husk temper, the phosphorus in these body prills could as well come from the temper. The need for these very specific conditions to be met and the limited mobility of the forming prills in the rigid ceramic fabric lead to the high compositional variability of the body prills (see Table 2).

Merv

The Merv crucibles[3] have a similar crucible profile as those from Telangana, but are structurally and compositionally different. The Merv crucibles are made of low-iron kaolinitic clay and are tempered with quartz and grog. No use of organic matter for tempering is reported or observed. The crucible FAG and base pad FAG is thinner than the FAG from the ferruginous crucibles of Telangana, as the kaolin-based clays are less susceptible to vitrification and glaze formation. In spite of its non-ferruginous clay nature, some iron prills do form in FAG, base pad FAG, base pad ceramic, crucible bodies and crucible slag. Most Merv prills are rather small and often at the limit of what can be analysed without 'contamination' from the surrounding matrix, as indicated in elevated levels of aluminium, oxygen and calcium in several of the analyses with elevated silicon (see Table 4). However, the phosphorus concentrations in FAG and body prills are certainly real, since the surrounding matrix does not contain significant amounts of P_2O_5. Overall, alloying elements found in the Merv prills include phosphorous and silicon and in addition nickel, arsenic, copper and tin, as well as sulfur. In contrast to the Telangana crucible prills, phosphorous is more prevalent here than silicon and the presence of non-ferrous metals is unique to Merv.

The source of silicon

Both the body and the FAG prills show some silicon enrichment, most likely from the reduction of some of the free silica in the ceramic, such as quartz particles (see

Table 4: Mgu 95 prill quartz periphery). The reduction of silica into silicon as an alloy with iron prills follows the same process as in the Telangana crucibles. However, the likelihood of it happening in the Merv crucible body prills is lower due to the lower iron oxide content in the ceramic and the absence of the highly siliceous rice husk temper. Thus, it appears mostly limited to the reaction of some quartz grains. While some silicon enrichment in FAG and body is analytically certain, some others, for instance in MGK 4 FAG (prill 1 and big crucible, c. body prill 1: see Table 4) could be an analytical contamination (see above). However, Feuerbach (2002, pp.96-99) has illustrated graphite flakes in one of the prills (prill A.4.2 B). While her data does not report any silicon, it is known that silicon in iron prills promotes the growth of graphite (grey cast iron) rather than cementite (white cast iron). Thus, the presence of graphite in some prills from Merv indicates that they did indeed contain silicon in the alloy.

The source of phosphorus

Some of the crucible body prills show high phosphorus enrichment, although not as much as in Telangana crucibles. In line with the lower bulk P_2O_5 content of Merv ceramic bodies (below the SEM-EDS detection limit) compared to Telangana (0.2 wt.%), prills with phosphorus enrichment are both few and very tiny, the reservoir of phosphorus being very little and limited. In contrast, the FAG prills show a high average phosphorus content (see Tables 2 and 4); as in the Telangana crucible FAG prills, this is likely due to the capture of phosphorus from the fuel ash during firing.

Non-ferrous alloying elements and sulfide prills

Most of the non-ferrous alloying elements are found in the crucible body prills, with an average of 1.5 wt.% nickel, 1 wt.% arsenic and 0.4 wt.% copper. Similar values were also found in some of the FAG prills, while the crucible slag prills only show a slightly elevated copper content, but none of the other elements (see Table 4).

The single base pad sample from Merv available for our study yielded numerous iron sulfide prills, both in the body and the FAG, containing up to about 10 wt.% copper and a small amount of arsenic. The pads are thought to serve to elevate the actual crucibles within the furnace chamber to sit above the fuel bed at the bottom (Feuerbach, 2002, p.111), implying that the pads themselves were embedded in the fuel and fuel ash. We think it unlikely that these copper- and sulfur-rich prills are the result of spilled crucible charge, e.g. from cracks in the vessels. Both copper and in particular sulfur are deleterious components in crucible steel, and sulfur has not been reported in any significant amounts in analysed crucible steel objects. Instead, given the desert oasis environment of Merv, it is more likely that the fuel ash contained a significant amount of sulfur; in addition, the soil itself is likely to contain significant amounts of gypsum, which under the strongly reducing conditions would be reduced to sulfide and bond with iron oxide from the soil to form these iron sulfide prills.

It is noteworthy that the Merv crucible slag/film prills contain far less of the non-ferrous alloying elements than the body and FAG prills; thus, the two main contaminants nickel and arsenic are likely not part of the metal charge. Instead, their presence in the ceramic bodies and the outer surfaces indicates that these two elements are from environmental contamination in the industrial area where the crucible workshop was found. Feuerbach (2002, p.101) offers the possibility of copper being added as crucible charge. This is a tempting assumption given the persistent copper quantification in the prills. However, this does not explain the Ni and As found in body and glaze prills, but not in crucible slag or base pad prills.

Manganese content in Merv crucible slags

The crucible slag in the Merv crucibles has MnO contents ranging from c 4 to about 15 wt.%. Despite this, the prills are more or less homogenous and show only very little uptake of Mn in the metal phase. This raises the question why MnO has been added to the crucible charge, where it affected the slag composition, but had no discernible alloying effect on the crucible slag prills and presumably the main ingot. This is in contrast to the observation in Güder, et al. (2022) who report up to 1.7 wt.% Mn in an ingot fragment and around 21 wt.% MnO in the attached slag, but consistent with the analyses in Alipour, Rehren and Martinón-Torres (2021) and Alipour and Rehren (2023) where prills embedded in high-MnO slag did not show elevated Mn content. It is thought (Rostoker and Bronson, 1990, pp.107-113; Truffaut, 2014) that MnO in slag facilitates carburisation of iron, even without contributing to the alloy itself. Thus, MnO could have been added to the charge to reduce the time needed to complete the crucible steel formation. Several reasons could then explain the variability in MnO in crucible slags, such as that taller crucibles and with heavier ingot output were supported by MnO based additives, whereas for smaller ingot sizes less MnO additive would be used, particularly if MnO was sparse or expensive. Alternatively, there could be different workshop practices, process-related variations, or time difference in production. The Ellingham diagram shows that reduction of MnO to Mn takes place once conditions are more reducing than needed for chromium reduction, but less reducing than

for silicon formation; thus, small variations in temperature and redox conditions may have played a major effect on whether MnO was reduced to the metallic state or not. This topic, however, is beyond the remit of this paper.

Prills: a representation of the ingot composition?

With very few exceptions (Jaikishan, Desai and Rehren, 2021; Güder, et al., 2022), the study of crucible steel production is restricted either to contemporary written sources, or the analysis of the production waste, while the ingots themselves are not available for characterisation. The composition of the ingots, however, plays a significant role in the literature (Verhoeven, Pendray and Dauksch, 2018; Wadsworth and Sherby, 1980; Alipour, Rehren and Martinón-Torres, 2021). This raises the question whether the prills identified here can be used as a proxy for the ingot composition. The prills across the crucible profile are compositionally highly variable. Clearly, the prills from the FAG/S with extremely high phosphorus or sulfur contents are unrelated to the ingot, since they have no mechanical connection to the crucible charge and form in chemically different environmental conditions. Similarly, the crucible body prills are more likely to represent the temper and the reducible clay components than the charge. In both these cases, the formation conditions are similar to that of the resulting ingot in terms of temperature and redox conditions, but differ in their chemical environment. The crucible slag prills have the same formation conditions and chemical environment as the ingot itself, yet, due to the difference in surface area and volume between the two and the surrounding silicate melt for the prills, the consolidation and alloy component enrichment patterns remain different. The slag covering the molten iron is likely to trap these molten prill droplets, preventing them from merging with the pool of liquid steel below. Alipour, Rehren and Martinón-Torres (2021) argue that the chromium-rich crucible slag prills in Chāhak broadly represent the assumed ingot composition, but in the absence of archaeologically surviving ingots from the site, no testable proof for this assertion is possible. The archaeological ingots recently made available from Telangana (Jaikishan, Desai and Rehren, 2021) are compositionally different to some of the crucible slag prills analysed here, in that the prills have higher phosphorus contents, while the ingots are pure carbon steels (Figure 28). Only the composition of Ind-Kp'19-Sl007 (see Table 2) and Ind-Ksm'19-sl002D (Figures 17b and 19) prills resembles closely the composition and microstructure of the ingots (see Figure 28) from Telangana. Further systematic work on crucible prills from multiple crucible steel production sites is required to discuss the representativity of the prills for the ingots and the crucible charge.

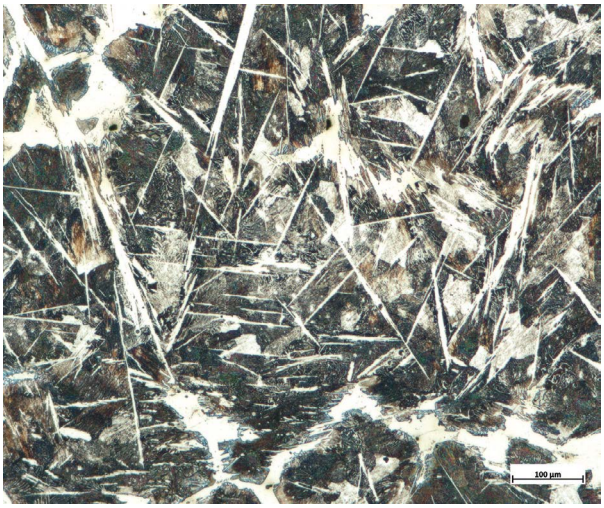

Figure 28. Etched optical micrograph at 100 µm of the crucible steel ingot from Konasamudram, Ing 32. The image shows grain boundary cementite and cementite lathes in a pearlite matrix and an average carbon content of around 2 wt.%. Photo: M. Desai and Th. Rehren, Archaeological Science Laboratories, The Cyprus Institute.

Conclusion

We analysed iron-based prills in crucible fragments from Telangana, India and Merv, Turkmenistan, which exploited ferruginous and kaolinitic clays, respectively, for crucible production. In most fragments of both crucible ceramics, prills were found in three distinct layers, namely in the FAG formed under the influence of the fuel ash from the furnace, the body of the crucibles and the crucible slag. Despite some degree of overlap in composition, we found systematic compositional differences between the prills formed in the three layers. We demonstrate that the local enrichments and microenvironments have a high degree of influence on prill formation and composition. The behaviour of NRCs differs greatly between bloomery smelting and crucible steel production, with their reducibility changing at the high temperature, longer firing times, element availability and strongly reducible conditions typical of the crucible steel process. The laws of Ellingham diagram are not fully obeyed in crucible steel production prills, but affected by the reaction kinetics. Iron prill formation and alloying occur irrespective of the crucible clay type, i.e. iron rich or iron deficit. However, the frequency, development and prominence of prills changes greatly, with ferruginous ceramics showing higher frequency of well-formed prills

occurring in the crucible matrix in contrast to iron poor ceramics.

The Telangana rice husk tempered crucibles with silica-rich phytoliths offer extra silicon to alloy with the body prills which can average around 10 wt.% silicon, the principle alloying element of Telangana body prills followed by phosphorus and carbon. The highly variable nature of silicon and phosphorus content in the prills reflects the microenvironments of the forming prills. In Telangana, this reflects the presence or absence of rice husk (silicon) and apatite mineral (phosphorus) close to the prill formation site. In Merv, silicon is only incorporated into the body prills near quartz grains, while the assumed addition of non-ferrous crucible waste as grog is likely responsible for the elevated nickel, copper and arsenic contents in some of the body prills.

The crucible FAG prills are a representation of the reducible fuel ash components, particularly phosphorus and, where present as in Merv, non-ferrous metals from general workshop contamination. Thus, neither of the prills formed in crucible body or FAG/S can represent the ingot composition, while only the crucible slag prills potentially represent the crucible charge. Analysed crucible slag prills should be further assessed for their relationship with the charge put into the crucible and not just the ingot removed from it at the end. A few crucible slag prills may represent the ingot composition, but due to heterogeneities among the prills the accuracy with which they represent the charge or the product is hard to determine. They may represent some exceptional or intermediate composition.

Overall, the metal prills within crucible steel crucibles provide a wealth of information regarding the original clay and its preparation, the temperature, redox and firing conditions of the process and those found in the crucible slag provide a first approximation of the compositional nature of the ingots produced. As so often, the data needs to be evaluated carefully and cannot be taken at face value, but still offer insights into the crafts people's choices and activities that are not available otherwise.

Acknowledgements

We thank Dr S. Jaikishan for providing us the access to the crucible fragments from Telangana and valuable insights on Telangana iron and steel production, including the fieldwork thereof. We warmly thank Drs St John Simpson and Ann Feuerbach for fragments from the crucibles from Merv for analysis, first conducted as part of Dr Feuerbach's doctoral research. We thank the State Archaeology Department, Telangana and the Export Authorities for permission to study the Telangana material. The analyses were done at the Cyprus Institute as part of the doctoral research of the first author. Financial support for her doctoral studies from the Gerda Henkel Foundation and from the A.G. Leventis Foundation for the operation of the laboratory to the first and second author, respectively, is gratefully acknowledged. Comments by the editor and two anonymous reviewers greatly enhanced the quality of the manuscript; all remaining errors are ours.

Notes

1 The discussion of the different production processes is an important topic, but for the current project, we focus on the observation and interpretation of prills, which are unrelated to the actual steel-making process. Production technology is discussed, e.g. by Rostoker and Bronson, 1981; Craddock, 1998; Juleff, 1998.

2 There is no archaeological record on the pre-firing of crucibles. The best and only description comes from S. Jaikishan and R. Balasubramaniam (2007), reporting an interview with wootz steel worker from Konapuram village in Northern Telangana. They mention shade drying of the crucibles for several days, but no pre-firing.

3 The Merv crucible steel making process has been interpreted variously over time as being either co-fusion (e.g. Feuerbach, et al., 1998; Merkel, 2013) or cementation (e.g. Feuerbach, 2002). Here is not the place to discuss this in depth, but we note the absence of cast iron production in Central Asia at the time in question, making co-fusion unlikely. The similarity of some Merv crucible slag compositions to early modern blast furnace slags reflects in our view not a similarity of process, but the similarity of process conditions, i.e. being reducing enough to reduce nearly all iron oxide from the melt to iron metal, irrespective of whether the carbon in the system comes from cast iron or added organic matter in the crucible.

References

Adeleke, A.A., Odusote, J.K., Ikubanni, P.P., Lasode, O.A., Malathi, M., Paswan, D. 2020. The ignitability, fuel ratio and ash fusion temperatures of torrefied woody biomass. *Heliyon,* 6(3), e03582. https://doi.org/10.1016/j.heliyon.2020.e03582.

Alipour, R., 2017. *Persian Crucible Steel Production: Chāhak Tradition*. Ph. D. University College London.

Alipour, R. and Rehren, Th., 2014. Persian pulād production: Chāhak tradition. *Journal of Islamic Archaeology,* 1(2), pp.231-261.

Alipour, R. and Rehren, Th., 2023. Archaeology and alchemy applied: experimental reproduction of Persian chromium crucible steel making. *Journal of Archaeological Science: Reports,* 47, 103814, pp.1-12.

Alipour, R., Rehren, Th. and Martinón-Torres, M., 2021. Chromium crucible steel was first made in Persia. *Journal of Archaeological Science,* 127, pp.1-14. https://doi.org/10.1016/j.jas.2020.105224.

Athira, G.B., Bahurudeen, A. and Appari, S., 2021. Rice-straw ash as a potential supplementary cementitious material: Influence of thermochemical conversion on its properties. *Journal of Material in Civil Engineering*, 33(6), p.04021123. https://ascelibrary.org/doi/10.1061/%28ASCE%29MT.1943-5533.0003727.

Balasubramaniam, R., Pandey, A. and Jaikishan, S., 2007. Analysis of wootz steel crucibles from Northern Telangana. *Indian Journal of History of Science*, 42, pp.649-671.

Bayley, J. and Rehren, Th., 2007. Towards a functional and typological classification of crucibles. In: S. La Niece, D. Hook and P.T. Craddock, ed. 2007. *Metals and Mines. Studies in Archaeometallurgy*. London: Archetype Books. pp.46-55.

Bui, D.D., Hu, J. and Stroeven, P, 2005. Particle size effect on the strength of rice husk ash blended gap-graded Portland cement concrete. *Cement & Concrete Composites,* 27, pp.357-366. https://doi.org/10.1016/j.cemconcomp.2004.05.002.

Charlton, M., Blakelock, E., Martinón-Torres, M. and Young, T., 2012. Investigating the production provenance of iron artefacts with multivariate methods. *Journal of Archaeological Science*, 39, pp. 2280-2293. https://doi.org/10.1016/j.jas.2012.02.037.

Chopra, D. and Siddique, R., 2015. Strength, permeability and microstructure of self-compacting concrete containing rice husk ash. *Biosystems Engineering*, 130, pp.72-80. https://doi.org/10.1016/j.biosystemseng.2014.12.005.

Craddock, P., 1998. New Light on the Production of Crucible Steel in Asia. *Bulletin of the Metals Museum*, 29, pp.41-66.

Desai, M., 2023. *Crucible steel making in Telangana*. Ph. D. The Cyprus Institute.

Desai, M. and Rehren, Th., forthcoming. Estimating carbon content in crucible steel using Image Analysis. *Historical Metallurgy*, accepted for publication.

Dillmann, P. and L'Héritier, M., 2007. Slag inclusion analyses for studying ferrous alloys employed in French medieval buildings: supply of materials and diffusion of smelting processes. *Journal of Archaeological Science*, 34(11), pp.1810-1823. https://doi.org/10.1016/j.jas.2006.12.022.

Feuerbach, A.M., Merkel, J.F. and Griffiths, D.R., 1998. An examination of crucible steel in the manufacture of Damascus steel, including evidence from Merv, Turkmenistan. In: Th. Rehren, A. Hauptmann and J. Muhly, eds. 1998. *Metallurgica Antiqua. In Honour of Hans-Gert Bachmann and Robert Maddin*. Bochum: Deutsches Bergbau-Museum. pp.37-44.

Feuerbach, A.M., 2002. *Crucible steel in Central Asia: production, use and origins.* Ph. D. University of London.

Freestone, I.C. and Tite, M.S., 1986. Refractories in the ancient and preindustrial world. In: W.D. Kingery and E. Lense, eds. 1986. *High-Technology Ceramics – Past, Present, and Future*. American Ceramic Society: Westerville, Ohio. pp.35-63.

Godfrey, E., 2007. *The Technology of Ancient and Medieval Directly Reduced Phosphoric Iron.* Ph. D. University of Bradford.

Ganesan, K., Rajagopal, K. and Thangavel, K., 2008. Rice husk ash blended cement: Assessment of optimal level of replacement for strength and permeability properties of concrete. *Construction and Building Materials*, 22(8), pp.1675-1683. https://doi.org/10.1016/j.conbuildmat.2007.06.011.

Girbal, B., 2017. *The Technological Context of Crucible Steel Production in Northern Telangana, India*. Ph. D. University of Exeter.

Güder, Ü., Çeken, M., Yavas, A., Yalçın, Ü. and Raabe, D., 2022. First evidence of crucible steel production in Medieval Anatolia, Kubadabad: A trace for possible technology exchange between Anatolia and Southern Asia. *Journal of Archaeological Science*, 137, p.105529. https://doi.org/10.1016/j.jas.2021.105529.

Ikpong, A.A. and Okpala, D.C., 1992. Strength characteristics of medium workability ordinary Portland cement-rice husk ash concrete. *Building and Environment*, 27(1), pp.105-111.

Jaikishan, S., 2007. Survey of iron and wootz steel production sites in northern Telangana. *Indian Journal of History of Science*, 42 (3), pp.445-460.

Jaikishan, S. and Balasubramaniam, R., 2007. Interview with wootz steel worker from Konapuram village in Northern Telangana. *Indian Journal of History of Science*, 42(4), pp.705-711.

Jaikishan, S., Desai, M. and Rehren, Th., 2021. A journey of over 200 years: early studies on wootz ingots and new evidence from Konasamudram, India. *Advances in Archaeomaterials***,** 2(1), pp.15-23. https://doi.org/10.1016/j.aia.2021.04.002.

Juleff, G., 1998. *Early Iron and Steel in Sri Lanka: A Study of the Samanalawewa Area*. AVA-Materialien 54: Mainz.

Juleff, G., Srinivasan, S. and Ranganathan, S., 2011. Pioneering Metallurgy: The origins of iron and steel making in the Southern Indian Subcontinent. *Telangana Field Survey Interim Report*. National Institute of Advanced Studies, Bangalore.

Kannan, V. and Ganesan, K., 2016. Effect of tricalcium aluminate on durability properties of self compacting concrete incorporating rice husk ash and metakaolin. *Journal of Material and Civil Engineering,* 28, pp.50-63. https://doi.org/10.1061/(ASCE)MT.1943-5533.0001330.

Lowe, T., 1989. Solidification and crucible processing of Deccani ancient steel. In: R. Trivedi, J.A. Shekhar and J. Mazumdar, eds. 1990, *Proceedings, Indo-US Conference on Principles of Solidification and Materials Processing*. Oxford and IBH: Delhi. pp.729-740.

Lowe, T., 1995. Indian iron ores and technology of Deccani wootz production. In: P. Benoit and P. Fluzin, eds. 1995. *Paleometallurgie du fer & Cultures*. Belfort-Sevenans: Vulcain. pp.119-129.

Lowe, T., Merk, N. and Thomas, G., 1990. An Historical Mullite Fiber-Reinforced Ceramic Composite: Characterization of the 'Wootz' Crucible Refractory. In: J.R. Druzik, P.B. Vandiver and G. Wheeler, eds. 1990. *Materials Issues*

in Art and Archaeology II. MRS Online Proceedings Library, 185. Pittsburgh: MRS. pp.627-632. https://doi.org/10.1557/PROC-185-627.

Martinón-Torres, M., Rehren, Th. and Freestone, I., 2006. Mullite and the Mystery of Hessian Wares. *Nature*, 444 (7118), pp.437-8. https://doi.org/10.1038/444437a.

Mehta, P.K., 1992. Rice husk ash – a unique supplementary cementing material. In: V.M. Malhotra, ed. 1992. *Proceedings of the International Symposium on Advances in Concrete Technology*. Athens, pp.407-430.

Memon, S.A., Shaikh, M.A. and Akbar, H., 2011. Utilization of rice husk ash as viscosity modifying agent in self compacting concrete. *Construction and Building Materials.,* 25, pp.1044-1048. https://doi.org/10.1016/j.conbuildmat.2010.06.074.

Merkel, J., 2013. New aspects of the 9th and 10th century Islamic period metallurgical workshop excavated at Merv, Turkmenistan: reassessing the slag compositions. In: J. Humphris and Th. Rehren, eds. 2013. *The World of Iron*. London: Archetype. pp.243-253.

Misra, M.K., Ragland, K.W. and Baker, A.J., 1993. Wood ash composition as a function of furnace temperature. *Biomass and Bioenergy*, 4(2), pp.103-116.

Neogi, T., 2017. *Technology and Identity: an ethnoarchaeological study of the social context of traditional iron-working in northern Telangana, India*. Ph. D. University of Exeter.

Pryce, T. and Natapintu, S., 2009. Smelting iron from laterite: Technical possibility or ethnographic aberration? *Asian Perspectives*, 48(2), pp.249-264.

Puigdollers, A.S., Schlexer, P., Tosoni, S. and Pacchioni, G., 2017. Increasing oxide reducibility: The role of metal/oxide interfaces in the formation of oxygen vacancies. *American Chemical Society Catalysis,* 7(10), pp.6493-6513. https://doi.org/10.1021/acscatal.7b01913.

Raheem, A.A. and Kareem, A.M., 2017. Chemical Composition and Physical Characteristics of Rice Husk Ash Blended Cement. *International Journal of Engineering Research in Africa,* 4(2), pp.25-35. https://doi.org/10.4028/www.scientific.net/JERA.32.25.

Reinmöller, M., Sieradzka, M., Laabs, M., Schreiner, M., Mlonka-Mędrala, A., Kopia, A., Meyer, B. and Magdziarz, A., 2021. Investigation of the thermal behaviour of different biomasses and properties of their low- and high-temperature ashes. *Fuel,* 301, p.121026.

Rehren, Th. and Papakhristu, O., 2000. Cutting edge technology - the Ferghana Process of medieval crucible steel smelting. *Metalla,* 7(2), pp.55-69.

Rehren, Th. and Papachristou, O., 2003. Similar like white and black: a comparison of steel–making crucibles from Central Asia and the Indian subcontinent. In: Th. Stöllner and G. Körlin, eds. 2003. *Man and Mining. Der Anschnitt, Beiheft*, 16. Bochum: Deutsches Bergbau-Museum. pp.393-404.

Rehren, Th. and Nixon, S., 2017. Crucible-steel making and other metalworking remains. In: S. Nixon ed. 2017. *Essouk – Tadmekka. An Early Islamic Trans-Saharan Market Town*, *Journal of African Archaeology Monograph Series*, 12. Leiden, Boston: Brill. pp.188-202.

Rostoker, W. and Bronson, B., 1990. *Pre-Industrial Iron – Its Technology and Ethnology*. Archeomaterials Monograph, 1. Philadelphia, PA: Archeomaterials.

Siddika, A., Abdullah Al Mamun, Md., Alyousef, R. and Hossein, M.H., 2021. State-of-the-art review on rice husk ash: A supplementary cementitious material in concrete. *Journal of King Saud University - Engineering Sciences,* 33(5), pp.294-307. https://doi.org/10.1016/j.jksues.2020.10.006.

Singh, B., 2018. Rice Husk Ash. In: R. Siddique and P. Cachim, eds. 2018. *Waste and Supplementary Cementitious Materials in Concrete*. Amsterdam: Elsevier. pp.417-460.

Srinivasan, S., 1994. Wootz crucible steel: a newly discovered production site in South India. *Papers from the Institute of Archaeology*, 5, pp.49-59.

Srinivasan, S. and Griffiths, D., 1997. Crucible steel in South India-Preliminary investigations on crucibles from some newly identified sites. In: P.B. Vandiver, J.R. Druzik, J.F. Merkel and J. Stewart, eds. 1997. *Materials Issues in Art and Archaeology-V*. *Materials Research Society Symposium Proceedings Series*, Vol 462. Pittsburgh: MRS. pp.111-125.

Stern, W.B. and Gerber, Y., 2004. Potassium-Calcium Glass: New Data and Experiments. *Archaeometry*, 46(1), pp.137-156.

Thiele, A., Török, B. and Költo, L., 2012. Energy dispersive X-ray analysis (SEM-EDS) on slag samples from medieval bloomery workshops – the role of phosphorus in the archaeometallurgy of iron in Somogy County, Hungary. In: D. Braekmans, J., Honings and P. Degryse, eds. 2012. *Proceedings of the 39th International Symposium for Archaeometry.* Leuven. pp.102-112.

Truffaut, E., 2014. Steelmaking in a bloomery furnace: behaviour of manganese. Research on the *Ferrum Noricum* process. In: B. Cech and Th. Rehren, eds. 2014. *Early Iron in Europe*. *Instrumentum Monographies*, 50. Montagnac: Éditions Monique Mergoil, pp.285-300.

Vega, E., Dillmann, P., L'Héritier, M., Fluzin, P., Crew, P. and Benoit, P., 2003. Forging of phosphoric iron. An analytical and experimental approach. In: Associazione Italiana di Metallurgia, ed. 2003. International Conference. *Archaeometallurgy in Europe*, *24-25-26 September 2003*. Vol. 1. Milan: AIM. pp.337-346.

Verhoeven, J.D., Pendray, A.H. and Dauksch, W.E., 2018. Damascus Steel Revisited. *Journal of Metals,* 70, pp.1331-1336. https://doi.org/10.1007/s11837-018-2915-z

Voysey, H.W., 1832. Description of the native manufacture of steel in Southern India. *Journal of Asiatic Society of Bengal*, 1, pp.245-247.

Wadsworth, J. and Sherby, O.D., 1980. On the Bulat—Damascus steels revisited. *Progress in Materials Science,* 25(3), pp.35-68**.** https://doi.org/10.1016/0079-6425(80)90014-6.

Zhang, M.H. and Malhotra, M.H., 1996. High-performance concrete incorporating rice husk ash as a supplementary cementing material. *ACI Materials Journal,* 93(6), pp.629-636.

Authors

Meghna Desai (Corresponding author)
The Science and Technology in Archaeology and Culture Research Center (STARC)
The Cyprus Institute, Nicosia-Aglantzia, Cyprus
m.desai@cyi.ac.cy

Sriperumbudur Jaikishan
Bhavan's New Science College
Hyderabad, India
dr.sjai@gmail.com

Thilo Rehren
The Science and Technology in Archaeology and Culture Research Center (STARC)
The Cyprus Institute, Nicosia-Aglantzia, Cyprus
th.rehren@cyi.ac.cy